Journal of Innovative Applied Mathematics and Computational Sciences

J. Innov. Appl. Math. Comput. Sci. **6**(1) (2026), 112–150. DOI: 10.58205/jiamcs.v6i1.2069

http://jiamcs.centre-univ-mila.dz/

A study on a modified fractional mathematical model of Listeria infection caused by pre-cooked packaged food by Homotopy analysis method

Sachin K N [1], Suguntha Devi K ✉[1] and Kumbinarasaiah S [1]

[1]Department of Mathematics, Bangalore University, Bengaluru, 560056, India

Received April 18, 2026, Accepted July 17, 2026, Published July 29, 2026

Abstract. This study examines the dynamics of a Listeria bacterium in a packaged food scenario using a mathematical framework that incorporates fractional derivatives in the Caputo sense. The model is solved using two primary methods: the homotopy analysis method (HAM), a semi-analytical approach that provides a series solution for fractional-order nonlinear ordinary differential equations (ODEs), and the Runge-Kutta 4th order (RK4) method, a well-known numerical technique for solving ODE systems. The HAM solution is derived by selecting a convergence control parameter, which produces a series of polynomials, whereas the RK4 method yields a fully numerical solution. The accuracy and dependability of both methods are evaluated by comparing their results to those of an ND Solver. The model's behavior under different parameter values is examined. All computations are carried out using Scilab and Mathematica software. The findings are presented in extensive graphs and tables, and formal theorems are used to demonstrate the convergence of the solution. This comparative method reveals the efficacy of fractional derivative modeling for analyzing bacterial activity in packaged food environments, as well as the effectiveness of HAM and RK4 in handling complex biological systems.

Keywords: Fractional calculus, ODE, Listeria infection model, HAM, Mathematical modeling.

2020 Mathematics Subject Classification: 26A33, 34A08, 65H20, 65T60. MSC2020

1 Introduction

Increased human populations and industrialization have made it more difficult for humanity to preserve the environment, which has caused disastrous effects on public health and significant ecological destruction. The growth in zoonotic diseases, including listeriosis, is one of the most severe issues [1]. Listeriosis is mainly acquired by eating contaminated food containing the bacterium Listeria monocytogenes. This dangerous public health issue primarily affects vulnerable groups, including aged people, infants, pregnant women, and people

✉Corresponding author. Email: suganthadevik77@gmail.com

ISSN (electronic): 2773-4196

with weakened immune systems [2,3]. On the other hand, it poses a significant risk to the health of both mothers and babies because it can be passed from mother to child through the skin or breathing system during childbirth. Numerous symptoms, such as fever, diarrhea, headaches, muscle aches, and nausea, are indicative of listeriosis [5]. Severe infections can result in dangerous blood infections called septicemia and meningitis, which is an infection of the membranes surrounding the brain and spinal cord [4]. Severe listeriosis is more likely to strike specific communities. Expectant mothers run the danger of miscarriage, stillbirth, early delivery, and infection in the unborn child, among other potentially disastrous results. In a similar vein, persons who are elderly or have compromised immune systems, such as those who have HIV/AIDS, cancer, or who are organ transplant recipients, are especially susceptible [6,7].

The main way to contract this illness is by eating contaminated food; common sources of infection include soft cheeses, hot dogs, deli meats, unpasteurized dairy products, and smoked fish [8,9]. Interestingly, Listeria monocytogenes is a common environmental pathogen that thrives in soil, water, and some animals. It may also multiply in foods stored in the refrigerator, posing a particular risk to food safety. However, prompt antibiotic treatment of listeriosis is essential, especially for individuals in high-risk groups [10]. Preventive actions are crucial to lower the risk of infection, including following excellent food safety practices. This includes washing fruits and vegetables, avoiding raw or unpasteurized dairy products, cooking meat and poultry completely, and ensuring food is handled safely to avoid cross-contamination [11]. There is a pressing need for efficient monitoring and intervention techniques due to the rising prevalence of listeriosis and its risks [12,13].

In various fields, mathematical modeling is an essential and flexible tool that enables us to investigate, evaluate, and address challenging real-world issues. In scholarly research and real-world applications, it is crucial to expand knowledge, improve decision-making, and encourage innovation. The power of mathematical modeling to use mathematical equations to represent and evaluate complex real-world occurrences makes it so important and provides insightful answers and forecasts [14–16]. Its applications in healthcare are wide-ranging and include medication development, therapy optimization, and disease spread prediction. Furthermore, it is essential in fields like systems biology, pharmacokinetics, and epidemiology [17,18].

Although conventional mathematical models have been beneficial in understanding the dynamics of infectious diseases, they frequently fail to capture the complex, time-dependent behaviors observed in real-world settings. We propose a fractional mathematical model that captures the non-integer-order behaviors common in biological systems to address this gap. Our model aims to provide a more detailed understanding of the transmission dynamics of listeriosis associated with the consumption of packaged foods by applying fractional calculus [19]. By accurately representing complicated behaviors and memory effects across a wide range of scientific and technical disciplines, fractional-order mathematical models improve upon conventional integer-order models [20,21].

Here, we employ the HAM to solve the model. The capacity of HAM, a potent analytical method, to solve complex differential equations, particularly fractional differential equations (FDEs), has recently attracted considerable interest. Non-integer-order derivatives (FDEs) are useful for modeling various phenomena in domains where typical integer-order models, such as physics, engineering, and finance, would not perform well. Because fractional derivatives are inherently complex, they pose special challenges that require the development of reliable solution techniques [22].

HAM is unique because it may be used to systematically and flexibly develop approximation solutions to nonlinear problems. HAM applies to a broader range of issues since it does not require small parameters, unlike conventional methods that frequently rely on perturbation techniques [23]. Using continuous deformation, this approach makes use of the homotopy idea to enable the transfer from a simple to a more complex problem [24, 25]. We can obtain precise and practical solutions that capture the complex behaviors typical of fractional dynamics by using HAM to FDEs. The approach improves comprehension of these equations and creates new opportunities to investigate their applicability in various technical and scientific fields. HAM is an essential tool for mathematicians and scientists working with FDEs as the need for efficient modeling of complicated systems grows [26, 27].

The rest of the paper is arranged as follows. Preliminaries of the HAM, fractional derivative, and convergence theorems are covered in Section 2. Section 3 provides a formulation for the Listeria model. The HAM for the system of FDEs is derived in Section 4. The solutions of the described model have been derived in Section 5. The numerical solutions obtained are presented in graphs and tables in Section 6. The conclusion is drawn in Section 7.

2 Preliminaries

Definition 2.1. Two continuous functions from one topological space to another are called homotopic if one can be continuously deformed into the other; such a deformation is called a homotopy between two functions.

Definition 2.2. Caputo time-fractional derivative of order $\beta > 0$ of $t(x)$ is defined as

$$D_t^{\beta}[t(x)] = \begin{cases} \frac{1}{\Gamma(n-\beta)} \int_0^x (x-\chi)^{n-\beta-1} \frac{\partial^n t(\chi)}{\partial \chi^n} d\chi, & n-1 < \beta < n, \\ \frac{\partial^n t(\chi)}{\partial \chi^n}, & \beta = n \in \mathbb{N}. \end{cases} \tag{2.1}$$

Theorem 2.3. *As long as the series $v_i(y) = \sum_{m=0}^{m} v_{i_m}(y)$ converges, it must be the exact solution of (4.1). Where $v_{i_m}(y)$ is governed by the m^{th} order deformation equation [33].*

Theorem 2.4. *Let $\psi_0, \psi_1, \psi_2, \ldots$ be the components of the solution of equation (4.1). The series solution $\sum_{k=0}^{\infty} \psi_k(t)$ converges if there exists $0 < \gamma < 1$ such that $||\psi_{k+1}|| \leq \gamma ||\psi_k||$, $\forall k \geq k_0$ for some $k_0 \in \mathbb{N}$ [32].*

Theorem 2.5. *Assume that the series solution $\sum_{k=0}^{\infty} \psi_k(t)$ is convergent to the solution $y(t)$. If the truncation series $\sum_{k=0}^{m} \psi_k(t)$ is the approximation to the solution $v_i(y)$, then the maximum absolute truncation error is calculated as*

$$||v_i(y) - \sum_{k=0}^{m} \psi_k(t)|| \leq \frac{1}{1-\gamma} \gamma^{m+1} ||\psi_0(t)||.$$

[32]

Theorem 2.6. *Suppose that the functions $D_*^{\alpha} v_i(y)$ are the approximation of $D_*^{\alpha} v_i(y)$ obtained using Haar wavelets. Then we have an exact upper bound as follows:*

$$||D_*^{\alpha} v_i(y) - D_*^{\alpha} v_{i,k}(y)||_E \leq \frac{M}{\Gamma(m-\alpha) \cdot (m-\alpha)} \frac{1}{[1-2^{2(\alpha-m)}]^{\frac{1}{2}}} \frac{1}{k^{m-\alpha}},$$

where $||v_i(y)||_E = \left(\int_0^1 (v_i)^2(y)dy\right)^{\frac{1}{2}}$ *[28].*

2.1 Non-negativity of solutions

Theorem 2.7. *For the fractional system (3.1) with initial conditions* $S(0) > 0$, $I(0) > 0$, $R(0) > 0$, $L_c(0) > 0$, $F_c(0) > 0$ *and* $F_u(0) > 0$, *all the solutions remain non-negative* $\forall t > 0$.

Proof. We use the generalized mean value theorem for Caputo fractional derivatives. If at any time t^*, a state variable reaches zero, we show that the Caputo derivative at that point is non-negative.

For $S(t)$**:** Suppose $S(t^*) = 0$ at some $t^* > 0$. Then

$$D^{\alpha}(S)\Big|_{S=0} = \mu_1 N + \rho R(t^*) \geq 0,$$

Since $\mu_1, N \geq 0$ and $R(t^*) \geq 0$ (both are non-negative biological parameters), hence $S(t)$ cannot decrease below zero.

For $I(t)$**:** If $I(t^*) = 0$, then

$$D^{\alpha}(I)\Big|_{I=0} = \vartheta_2 L_c(t^*)S(t^*) \geq 0.$$

For $R(t)$**:** If $R(t^*) = 0$, then

$$D^{\alpha}(R)\Big|_{R=0} = \delta I(t^*) \geq 0.$$

For $L_c(t)$**:** If $L_c(t^*) = 0$, then

$$D^{\alpha}(L_c)\Big|_{L_c=0} = -\eta_1 I(t^*).$$

For this to remain non-negative, it requires $\eta_1 I(t^*) = 0$. Since η_1 is the antibiotic rate, this condition holds when the infected population is zero ($I = 0$) or when antibiotics are not applied. Biologically, this is consistent with an early outbreak scenario where bacterial growth dominates antibiotic clearance.

For $F_c(t)$**:** If $F_c(t^*) = 0$, then

$$D^{\alpha}[F_c(t)]\Big|_{F_c=0} = \vartheta_2 F_u(t^*) \geq 0.$$

For $F_u(t)$**:** If $F_u(t^*) = 0$, then

$$D^{\alpha}[F_u(t)]\Big|_{F_u=0} = \mu_2 F_c(t^*) \geq 0.$$

Therefore, the non-negative orthant $\mathbb{R}^6_+$ is positively invariant for system (3.1). All biologically meaningful solutions remain non-negative $\forall t > 0$. □

2.2 Boundedness of solutions

Theorem 2.8. *All solutions of system (3.1) initiating in* $\mathbb{R}^6_+$ *are uniformly bounded* $\forall t > 0$.

Proof. Let the total human population be $N(t) = S(t) + I(t) + R(t)$. From the first three equations of (3.1):

$$\begin{aligned} D^{\alpha}(N) = &\mu_1 N + \rho R(t) - \vartheta_1 S(t) I(t) - \mu_1 S(t) - \vartheta_2 L_c(t) S(t) \\ &+ \vartheta_1 S(t) I(t) - \delta I(t) - \mu_1 I(t) + \vartheta_2 L_c(t) S(t) \\ &+ \delta I(t) - \rho R(t) - \mu_1 R(t), \end{aligned}$$

$$D^{\alpha}(N) = \mu_1 N - \mu_1 (S + R + I) = \mu_1 N - \mu_1 N = 0.$$

This shows that $D^{\alpha}(N) = 0$, meaning $N(t) = N(0) = \text{constant } \forall t > 0$. The total human population is invariant, so S, I, R are bounded above by $N(0)$.

For $L_c(t)$: From $D^{\alpha}(L_c) = \eta L_c - \eta_1 I$, and given that I is bounded by N:

$$D^{\alpha}(L_c) \leq \gamma L_c.$$

By the comparison theorem for fractional ODEs:

$$L_c(t) \leq L_c(0) E_{\alpha}(\eta t^{\alpha}),$$

where E_{α} is the Mittag-Leffler function. This shows $L_c(t)$ grows but remains bounded over any finite time interval $[0, T]$. □

2.3 Disease-free equilibrium (DFE)

At the DFE, the disease is absent: $I^* = 0$ and $L_c^* = 0$. Setting all Caputo derivatives to zero in system (3.1):

2.3.1 Food compartments

From the F_c and F_u equations with $L_c = 0$:

$$\vartheta_2 F_u^* - \mu_2 F_c^* = 0 \quad \text{and} \quad F_u^* + F_c^* = F_0.$$

Solving simultaneously yields:

$$F_c^* = \frac{\vartheta_2 F_0}{\vartheta_2 + \mu_2}, \quad F_u^* = \frac{\mu_2 F_0}{\mu_2 + \vartheta_2}.$$

2.3.2 Human compartments

From the R equation with $I^* = 0$, we get $R^* = 0$. From the S equation with $R^* = 0, L_c^* = 0$, and $I^* = 0$:

$$\mu_1 N - \mu_1 S^* = 0 \implies S^* = N.$$

2.3.3 DFE vector

The Disease-Free Equilibrium point is given by:

$$E_0 = \left(N, 0, 0, 0, \frac{\vartheta_2 F_0}{\vartheta_2 + \mu_2}, \frac{\mu_2 F_0}{\mu_2 + \vartheta_2} \right).$$

2.4 Existence and uniqueness

Theorem 2.9. *The solution of the considered model (3.1) exists and is unique in the region* $A \times [0, T]$, *where:*

$$A = (S, I, R, L_c, F_c, F_u) \in \mathbb{R}^6 :$$

$\|S\| \leq k_1, \quad \|I\| \leq k_2, \quad \|R\| \leq k_3, \quad \|L_c\| \leq k_4, \quad \|F_c\| \leq k_5, \quad \|F_u\| \leq k_6$ *and* $T < \infty$.

Proof. Let $U(t) = (S(t), I(t), R(t), L_c(t), F_c(t), F_u(t))$ and $\overline{U}(t) = (\overline{S}(t), \overline{I}(t), \overline{R}(t), \overline{L}_c(t), \overline{F}_c(t), \overline{F}_u(t))$.

Consider a function Z on $A \times [0, T]$ and its decomposed form as:

$$Z(U, t) = (Z_1(U, t), Z_2(U, t), Z_3(U, t), Z_4(U, t), Z_5(U, t), Z_6(U, t))$$

where:

$$\begin{aligned}
Z_1(U, t) &= \mu_1 N + \beta R - \nu_1 SI - \mu_1 S - \nu_2 L_c S, \\
Z_2(U, t) &= \nu_1 SI - \gamma I - \mu_1 I + \nu_2 L_c S, \\
Z_3(U, t) &= \gamma I - \beta R - \mu_1 R, \\
Z_4(U, t) &= \eta L_c - \eta_1 I, \\
Z_5(U, t) &= \vartheta_2 F_u - \mu_2 F_c, \\
Z_6(U, t) &= -\vartheta_2 F_u + \mu_2 F_c.
\end{aligned}$$

Norm is taken as:

$$\|U(t)\| = \sup_{t \in [0,T]} |U(t)| \quad \text{and} \quad m = \sup_A \|Z(U, t)\|.$$

Consider

$$\begin{aligned}
&\|Z(U, t) - Z(\overline{U}, t)\| \\
&= \Big\| \Big(\mu_1 N + \beta R - \nu_1 SI - \mu_1 S - \nu_2 L_c S\Big) - \Big(\mu_1 N + \beta \overline{R} - \nu_1 \overline{S}\,\overline{I} - \mu_1 \overline{S} - \nu_2 \overline{L}_c \overline{S}\Big), \\
&\Big(\nu_1 SI - \gamma I - \mu_1 I + \nu_2 L_c S\Big) - \Big(\nu_1 \overline{S}\,\overline{I} - \gamma \overline{I} - \mu_1 \overline{I} + \nu_2 \overline{L}_c \overline{S}\Big), \\
&\Big(\gamma I - \beta R - \mu_1 R\Big) - \Big(\gamma \overline{I} - \beta \overline{R} - \mu_1 \overline{R}\Big), \\
&\Big(\eta L_c - \eta_1 I\Big) - \Big(\eta \overline{L}_c - \eta_1 \overline{I}\Big), \\
&\Big(\vartheta_2 F_u - \mu_2 F_c\Big) - \Big(\vartheta_2 \overline{F}_u - \mu_2 \overline{F}_c\Big) \Big\| \\
&\leq (-\nu_1 k_2 - \mu_1 - \nu_2 k_4) \|S - \overline{S}\| + (\nu_1 k_1 - \gamma - \mu_1) \|I - \overline{I}\| \\
&+ (-\beta - \mu_1) \|R - \overline{R}\| + \eta \|L_c - \overline{L}_c\| + \mu_2 \|F_c - \overline{F}_c\| - \vartheta_2 \|F_u - \overline{F}_u\|.
\end{aligned}$$

This implies

$$\begin{aligned}
\|Z(U, t) - Z(\overline{U}, t)\| \leq{}& \varphi_1 \|S - \overline{S}\| + \varphi_2 \|I - \overline{I}\| + \varphi_3 \|R - \overline{R}\| \\
&+ \varphi_4 \|L_c - \overline{L}_c\| + \varphi_5 \|F_c - \overline{F}_c\| + \varphi_6 \|F_u - \overline{F}_u\|,
\end{aligned}$$

where:

$$\begin{aligned}
\varphi_1 &= -\nu_1 k_2 - \mu_1 - \nu_2 k_4, \\
\varphi_2 &= \nu_1 k_1 - \gamma - \mu_1, \\
\varphi_3 &= -\beta - \mu_1, \\
\varphi_4 &= \eta, \\
\varphi_5 &= \mu_2, \\
\varphi_6 &= -\vartheta_2.
\end{aligned}$$

We obtain:

$$\Psi = \max\{\varphi_1, \varphi_2, \varphi_3, \varphi_4, \varphi_5, \varphi_6\} + \omega_{01},$$

$$\|Z(U,t) - Z(\overline{U},t)\| \leq \Psi \|U - \overline{U}\|.$$

This equation represents Lipschitz continuity of $Z(U,t)$. We obtain the following equation by constructing a Picard operator Δ using the function Z, and fractional integral:

$$\Delta U = U(0) + I^{\alpha} Z(U,t). \tag{2.2}$$

Now, we want to show that Δ is a contraction operator, i.e., Δ contracts the distance between points in the metric space.

Consider:

$$\|U^{(t)} - U(0)\| < \beta.$$

From Eqn (2.2):

$$\|U(t) - U(0)\| \leq I^{\alpha} \|Z(U,t)\| \leq \frac{T^{\alpha}}{\Gamma(\alpha+1)} m < \beta.$$

Again,

$$\begin{aligned}
\|\Delta U - \Delta \overline{U}\| &= \|I^{\alpha}\Big(Z(U,t) - Z(\overline{U},t)\Big)\| \\
&\leq I^{\alpha} \|Z(U,t) - Z(\overline{U},t)\| \\
&\leq \frac{T^{\alpha}}{\Gamma(\alpha+1)} \Psi \|U - \overline{U}\|.
\end{aligned}$$

Taking $\frac{T^{\alpha}}{\Gamma(\alpha+1)} \Psi = \phi$, we get:

$$\|\Delta U - \Delta \overline{U}\| \leq \phi \|U - \overline{U}\|.$$

This shows that Δ is a contraction mapping. Therefore, Δ possesses a unique fixed point. Hence, by the Banach fixed-point theorem, the fractional differential equation given by (3.1) possesses a unique solution. □

Note: Throughout this work, ND Solve refers to the built-in numerical differential equation solver in Wolfram Mathematica, which adaptively selects and applies appropriate numerical algorithms to solve systems of differential equations to high precision. It serves as the benchmark for all comparisons presented in this study.

3 Model formulation

The modified mathematical model of Listeria infection caused by pre-cooked packaged food contains three phases: human population, Listeria population in the surroundings, and pre-cooked packaged food. The human population is further divided into Susceptible $S(t)$, infected $I(t)$ and recovered population $R(t)$. The total population N is the sum of these compartments, i.e. $N(t) = S(t) + I(t) + R(t)$. The pre-cooked packaged foods include both contaminated food F_c and uncontaminated food F_u. L_c is the Listeria bacteria population. The term $-\eta_1 I(t)$ models the indirect reduction of the environmental Listeria bacterial population due to antibiotic treatment administered to infected individuals, which reduces bacterial shedding into the environment, and the removal of infected individuals from food-handling activities. The parameter $\eta_1 > 0$ quantifies this combined reduction rate. The detailed descriptions of the parameters used to describe the model are given in Table 3.1.

We developed a fractional mathematical model for the Listeria infection caused by pre-cooked packaged food by applying the Caputo-fractional derivative as follows [29]:

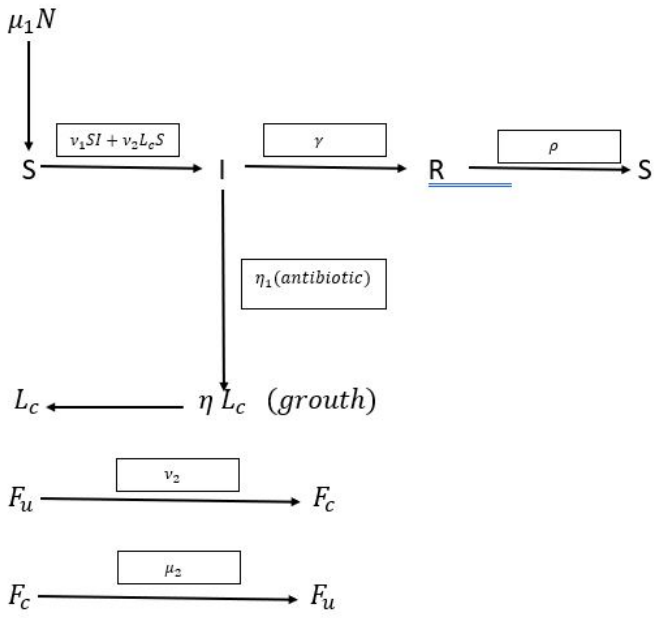

Figure 3.1: Flow diagram of the model.

Table 3.1: Descriptions of the parameters presented in the model.

Parameter	Description
μ_1	Mortality rate of each class of population
μ_2	Convergence rate from uncontaminated food to contaminated food
ρ	Recovered rate
ν_1	Infection rate
γ	Recovery rate
η	Growth rate of L_c
ν_2	Infection rate of L_c to S
η_1	Rate of antibiotic given to infected population

$\mu_1 N \to S$	Recruitment of susceptible population
$\vartheta_1 SI \to I$	Human to human infection transmission
$\vartheta_2 L_c S \to I$	Environment to human infection via Listeria
$\gamma I \to R$	Recovery of infected individuals
$\rho R \to S$	Return to susceptible class
ηL_c	Natural growth of Listeria in environment
$\eta_1 I \to L_c$	Reduction of Listeria due to antibiotic treatment
$\vartheta_2 F_u \to F_c$	Contamination of uncontaminated food
$\mu_2 F_c \to F_u$	Decontamination of contaminated food

$$\begin{cases} D^{\alpha}[S(t)] = \mu_1 N + \rho R(t) - \nu_1 S(t) I(t) - \mu_1 S(t) - \nu_2 L_c(t) S(t), \\ D^{\alpha}[I(t)] = \nu_1 S(t) I(t) - \gamma I(t) - \mu_1 I(t) + \nu_2 L_c(t) S(t), \\ D^{\alpha}[R(t)] = \gamma I(t) - \rho R(t) - \mu_1 R(t), \\ D^{\alpha}[L_c(t)] = \eta L_c(t) - \eta_1 I(t), \\ D^{\alpha}[F_c(t)] = \nu_2 F_u(t) - \mu_2 F_c(t), \\ D^{\alpha}[F_u(t)] = -\nu_2 F_u(t) + \mu_2 F_c(t). \end{cases} \tag{3.1}$$

Human population dynamics

- **Susceptible Individuals,** $S(t)$**:** Individuals who are healthy but at risk of contracting listeriosis through the consumption of contaminated pre-cooked packaged food or through exposure to Listeria monocytogenes present in the environment. The susceptible population is replenished through recruitment at a rate $\mu_1 N$ and by the loss of immunity in recovered individuals at a rate ρ.

- **Infected Individuals,** $I(t)$**:** Individuals who have contracted listeriosis. Infection occurs through two pathways: (i) direct contact with infected individuals at transmission rate ν_1, and (ii) exposure to environmental Listeria bacteria at transmission rate ν_2. Infected individuals recover at a rate γ or leave the population through natural mortality and disease-induced mortality at a rate μ_1.

- **Recovered Individuals,** $R(t)$**:** Individuals who have recovered from listeriosis infection. Since immunity is assumed to be temporary, recovered individuals lose immunity and return to the susceptible class at a rate ρ. This assumption reflects the observation that immunity to listeriosis is not permanent, particularly among immunocompromised individuals.

Environmental bacterial dynamics

- **Environmental Listeria Population,** $L_c(t)$**:** Represents the environmental reservoir of Listeria monocytogenes. The bacterial population grows logistically at intrinsic growth rate η, capturing its ability to proliferate in refrigerated environments and food-processing facilities. The term $-\eta_1 I(t)$ models the indirect reduction of the environmental bacterial population due to antibiotic treatment of infected individuals and their removal from food-handling activities. The parameter $\eta_1 > 0$ denotes the corresponding reduction rate.

Food compartment dynamics

- **Contaminated Food,** $F_c(t)$**:** Pre-cooked packaged food products contaminated with Listeria monocytogenes through environmental exposure, cross-contamination during processing, or improper storage. Contamination occurs from the uncontaminated food compartment at a rate ν_2.
- **Uncontaminated Food,** $F_u(t)$**:** Pre-cooked packaged food products free from Listeria monocytogenes contamination. These products become contaminated at a rate ν_2 and are replenished through decontamination processes acting on contaminated food at a rate μ_2.

4 Method of solution

4.1 Homotopy analysis method

Consider the nonlinear system of FDEs of the type [30]:

$$\mathscr{D}^{\beta}[s_i(t)] = \mathscr{G}_i(t, s_1, s_2, \ldots, s_n), \quad i = 1, 2, 3, \ldots, n, \quad 0 < \beta \leq 1, \quad t \geq 0, \tag{4.1}$$

subject to the condition:

$$s_i = a_i, \qquad i = 1, 2, 3, \ldots, n. \tag{4.2}$$

Where $\mathscr{D}^{\beta}$ is the fractional differential operator of β^{th} order, and $s_i(t)$ are the functions to be found.

Zeroth order deformation equation:

Let $s_{i_0}(t)$ be the initial approximation to the actual solution of (4.1) for $i = 1, 2, 3, \ldots, n$. Taking auxiliary functions $\mathscr{H}(t)(\neq 0)$ and auxiliary parameter $\hat{h}(\neq 0)$, the zeroth order deformation equations are defined as [31]:

$$(1-q)\mathscr{L}_i[\varphi_i(t;q) - s_{i_0}(t)] = q\hat{h}\mathscr{H}(t)\mathscr{G}_i[\varphi_i(t;q)], \quad i = 1, 2, 3, \ldots, n. \tag{4.3}$$

subject to the conditions:

$$\varphi_i(0;q) = a_i, \quad i = 1, 2, 3, \ldots, n. \tag{4.4}$$

where $\varphi_i(t;q)$ are unknown functions, and $\mathscr{L}_i$ are the linear operators.

At $q = 0$, (4.3) becomes $\varphi_i(t;0) = s_{i_0}(t)$ and at $q = 1$, (4.3) becomes $\varphi_i(t;1) = s_i(t)$. So $\varphi_i(t;q)$ varies from initial approximation $s_{i_0}(t)$ to the actual solution $s_i(t)$, $i = 1, 2, 3, \ldots, n$, as q varies from 0 to 1.

Defining derivatives of the m^{th} order deformation:

$$s_{i_m}(t) = \frac{1}{m!}\frac{\partial^m \varphi_i(t;q)}{\partial q^m}, \quad i = 1, 2, 3, \ldots, n. \tag{4.5}$$

Taylor series expansion of $\varphi_i(t;q)$ with respect to q, $i = 1, 2, 3, \ldots, n$, is:

$$\varphi_i(t;q) = s_{i_0}(t) + \sum_{m=1}^{\infty} s_{i_m}(t)q^m, \quad i = 1, 2, 3, \ldots, n. \tag{4.6}$$

As we know $\varphi_i(t;q)$ becomes the required solution at $q = 1$, equation (4.6) becomes:

$$\varphi_i(t;1) = s_i(t) = s_{i_0}(t) + \sum_{m=1}^{\infty} s_{i_m}(t), \quad i = 1, 2, 3, \ldots, n. \tag{4.7}$$

In a similar way, the m^{th} order deformation equations are obtained as:

$$\mathscr{L}[s_{i_m}(t) - \chi_m s_{i_{m-1}}(t)] = \hat{h}\mathscr{H}(t)\mathscr{R}_{i,m}(s_{i_{m-1}}(t)), \quad i = 1,2,3,\ldots,n. \tag{4.8}$$

where

$$\chi_m = \begin{cases} 0 & \text{if } m \leq 1, \\ 1 & \text{Otherwise.} \end{cases} \tag{4.9}$$

$$\mathscr{R}_{i,m}(s_{i_{m-1}}(t)) = \frac{1}{(m-1)!}\frac{\partial^{m-1}[\mathscr{G}[\varphi_i(t;q)]]}{\partial q^{m-1}}, \quad i = 1,2,3,\ldots,n. \tag{4.10}$$

Thus solving equation (4.8) we can get $s_{i_1}(t)$, $s_{i_2}(t)$, $s_{i_3}(t)$, ...
The m^{th} order approximation of $s_i(t)$ [33–35] is given by:

$$s_i(t) = \sum_{m=0}^{m} s_{i_m}(t). \tag{4.11}$$

Equation (4.11) is the semi-analytical solution of (4.1).

5 Solution of the modified fractional mathematical model of Listeria infection caused by pre-cooked packaged food

Consider the modified packed food model:

$$\begin{cases} D^{\alpha}[S(t)] = \mu_1 N + \rho R(t) - \nu_1 S(t)I(t) - \mu_1 S(t) - \nu_2 L_c(t)S(t), \\ D^{\alpha}[I(t)] = \nu_1 S(t)I(t) - \gamma I(t) - \mu_1 I(t) + \nu_2 L_c(t)S(t), \\ D^{\alpha}[R(t)] = \gamma I(t) - \rho R(t) - \mu_1 R(t), \\ D^{\alpha}[L_c(t)] = \eta L_c(t) - \eta_1 I(t), \\ D^{\alpha}[F_c(t)] = \nu_2 F_u(t) - \mu_2 F_c(t), \\ D^{\alpha}[F_u(t)] = -\nu_2 F_u(t) + \mu_2 F_c(t). \end{cases} \tag{5.1}$$

With initial conditions:

$$S(0) = S_0, \quad I(0) = I_0, \quad R(0) = R_0, \quad L_c(0) = L_{c_0}, \quad F_c(0) = F_{c_0}, \quad F_u(0) = F_{u_0}. \tag{5.2}$$

The parameter values are taken as $\mu_1 = 0.0001$, $\mu_2 = \frac{1}{65\times 360}$, $\rho = 0.1$, $\nu_1 = 0.005$, $\gamma = 0.05$, $\eta = 0.01$, $\nu_2 = 0.01$, $\eta_1 = 0.01$. The initial values are taken as $S(0) = 60$, $I(0) = 2$, $R(0) = 1$, $L_c(0) = 0.2 \times \log(10)$, $F_c(0) = 30$ and $F_u(0) = 1$.

Applying HAM to (5.1) and (5.2), according to (4.3), the zeroth order deformation is given by:

$$\begin{aligned}
(1-q)\mathscr{L}_1[\varphi_1(t;q) - S_0(t)] &= q\hat{h}\mathscr{H}(t)[D^{\alpha}\varphi_1(t;q) - \mu_1 N - \rho\varphi_3(t;q) + \nu_1\varphi_1(t;q)\varphi_2(t;q) \\
&\quad +\mu_1\varphi_1(t;q) + \nu_2\varphi_4(t;q)\varphi_1(t;q)], \\
(1-q)\mathscr{L}_2[\varphi_2(t;q) - I_0(t)] &= q\hat{h}\mathscr{H}(t)[D^{\alpha}\varphi_2(t;q) - \nu_1\varphi_1(t;q)\varphi_2(t;q) + \gamma\varphi_2(t;q) + \mu_1 I(t) \\
&\quad -\nu_2\varphi_4(t;q)\varphi_1(t;q)], \\
(1-q)\mathscr{L}_3[\varphi_3(t;q) - R_0(t)] &= q\hat{h}\mathscr{H}(t)[D^{\alpha}\varphi_3(t;q) - \gamma\varphi_2(t;q) + \rho\varphi_3(t;q) + \mu_1\varphi_3(t;q)], \\
(1-q)\mathscr{L}_4[\varphi_4(t;q) - L_{c_0}(t)] &= q\hat{h}\mathscr{H}(t)[D^{\alpha}\varphi_4(t;q) - \eta\varphi_4(t;q) + \eta_1\varphi_2(t;q)], \\
(1-q)\mathscr{L}_5[\varphi_5(t;q) - F_{c_0}] &= q\hat{h}\mathscr{H}(t)[D^{\alpha}\varphi_5(t;q) - \nu_2\varphi_6(t;q) + \mu_2\varphi_5(t;q)], \\
(1-q)\mathscr{L}_6[\varphi_6(t;q) - F_{u_0}(t)] &= q\hat{h}\mathscr{H}(t)[D^{\alpha}\varphi_6(t;q) + \nu_2\varphi_6(t;q) - \mu_2\varphi_5(t;q)].
\end{aligned} \tag{5.3}$$

Taking $\mathscr{H}(t) = 1$, the m^{th} order deformations are given by:

$$\begin{aligned}
D^{\alpha}[S_m(t) - \chi_m S_{m-1}(t)] &= \hat{h}\mathscr{R}_{1,m}(S_{m-1}(t)),\\
D^{\alpha}[I_m(t) - \chi_m I_{m-1}(t)] &= \hat{h}\mathscr{R}_{2,m}(I_{m-1}(t)),\\
D^{\alpha}[R_m(t) - \chi_m R_{m-1}(t)] &= \hat{h}\mathscr{R}_{3,m}(R_{m-1}(t)),\\
D^{\alpha}[L_{c_m}(t) - \chi_m L_{c_{m-1}}(t)] &= \hat{h}\mathscr{R}_{4,m}(L_{c_{m-1}}(t)),\\
D^{\alpha}[F_{c_m}(t) - \chi_m F_{c_{m-1}}(t)] &= \hat{h}\mathscr{R}_{5,m}(F_{c_{m-1}}(t)),\\
D^{\alpha}[F_{u_m}(t) - \chi_m F_{u_{m-1}}(t)] &= \hat{h}\mathscr{R}_{6,m}(F_{u_{m-1}}(t)).
\end{aligned} \tag{5.4}$$

Subject to:

$$S_m(0) = 0, \quad I_m(0) = 0, \quad R_m(0) = 0, \quad L_{c_m}(0) = 0, \quad F_{c_m}(0) = 0, \quad F_{u_m}(0) = 0, \quad m \geq 1. \tag{5.5}$$

Where

$$\begin{aligned}
\mathscr{R}_{1,m}(S_{m-1}(t)) &= D^{\alpha}[S_{m-1}(t)] - (1-\chi_m)\mu_1 N - \rho R_{m-1}(t) + \nu_1 \sum_{j=0}^{m-1} S_j(t) I_{m-1-j}(t)\\
&\quad + \mu_1 S(t) + \nu_2 \sum_{j=0}^{m-1} L_{c_j}(t) S_{m-1-j}(t),\\
\mathscr{R}_{2,m}(I_{m-1}(t)) &= D^{\alpha}[I_{m-1}(t)] - \nu_1 \sum_{j=0}^{m-1} S_j(t) I_{m-1-j}(t) + \gamma I_{m-1}(t) + \mu_1 I_{m-1}(t)\\
&\quad - \nu_2 \sum_{j=0}^{m-1} L_{c_j}(t) S_{m-1-j}(t),\\
\mathscr{R}_{3,m}(R_{m-1}(t)) &= D^{\alpha}[R_{m-1}(t)] - \gamma I_{m-1}(t) + \rho R_{m-1}(t) + \mu_1 R_{m-1}(t),\\
\mathscr{R}_{4,m}(L_{c_{m-1}}(t)) &= D^{\alpha}[L_{c_{m-1}}(t)] - \eta L_{c_{m-1}}(t) + \eta_1 I_{m-1}(t),\\
\mathscr{R}_{5,m}(F_{c_{m-1}}(t)) &= D^{\alpha}[F_{c_{m-1}}(t)] - \nu_2 F_{u_{m-1}}(t) + \mu_2 F_{c_{m-1}}(t),\\
\mathscr{R}_{6,m}(F_{u_{m-1}}(t)) &= D^{\alpha}[F_{u_{m-1}}(t)] + \nu_2 F_{u_{m-1}}(t) - \mu_2 F_{c_{m-1}}(t).
\end{aligned} \tag{5.6}$$

Applying J^{α}, the inverse of D^{α}, on both sides of (5.4), we get:

$$\begin{aligned}
S_m(t) &= \chi_m S_{m-1}(t) + \hat{h} J^{\alpha}[\mathscr{R}_{1,m}(S_{m-1}(t))] + C_1,\\
I_m(t) &= \chi_m I_{m-1}(t) + \hat{h} J^{\alpha}[\mathscr{R}_{2,m}(I_{m-1}(t))] + C_2,\\
R_m(t) &= \chi_m R_{m-1}(t) + \hat{h} J^{\alpha}[\mathscr{R}_{3,m}(R_{m-1}(t))] + C_3,\\
L_{c_m}(t) &= \chi_m L_{c_{m-1}}(t) + \hat{h} J^{\alpha}[\mathscr{R}_{4,m}(L_{c_{m-1}}(t))] + C_4,\\
F_{c_m}(t) &= \chi_m F_{c_{m-1}}(t) + \hat{h} J^{\alpha}[\mathscr{R}_{5,m}(F_{c_{m-1}}(t))] + C_5,\\
F_{u_m}(t) &= \chi_m F_{u_{m-1}}(t) + \hat{h} J^{\alpha}[\mathscr{R}_{6,m}(F_{u_{m-1}}(t))] + C_6, \quad m \geq 1.
\end{aligned} \tag{5.7}$$

C_1, C_2, C_3, C_4, C_5 and C_6 are calculated using (5.5).
The HAM solutions at $\hat{h} = -1$ for integer $\alpha(= 1)$ are:

$$S(t) = \sum_{m=0}^{m} S_m(t) = 60 + t(-0.776182 + (-0.0489748 + 0.00677743t)t + \cdots),$$
$$I(t) = \sum_{m=0}^{m} I_m(t) = 2 + t(0.776225 + (0.029567 - 0.00662302t)t) + \cdots,$$
$$R(t) = \sum_{m=0}^{m} R_m(t) = 1 + t(-0.000042735 + (0.0194078 - 0.000154418t)t) + \cdots,$$
$$L_c(t) = \sum_{m=0}^{m} L_{c_m}(t) = 0.460517 + t(-0.205921 + (-0.0418835 - 0.00117705t)t) + \cdots,$$
$$F_c(t) = \sum_{m=0}^{m} F_{c_m}(t) = 30 + t(-0.29 + (0.0029 - 0.0000193333t)t) + \cdots,$$
$$F_u(t) = \sum_{m=0}^{m} F_{u_m}(t) = 1 + t(0.29 + (-0.0029 + 0.0000193333t)t) + \cdots.$$

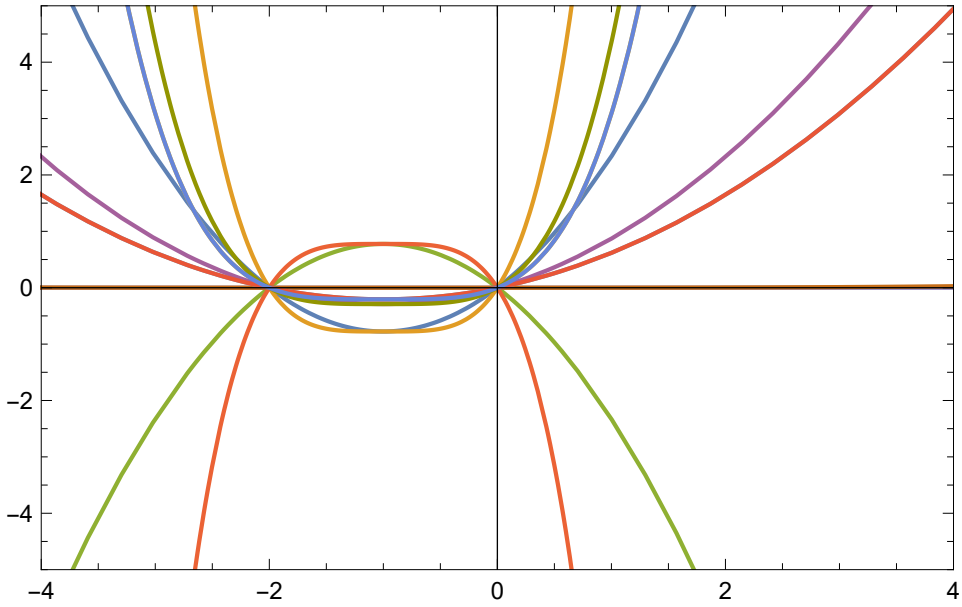

Figure 5.1: $\hat{h}$-curves for the Listeria model.

Each curve represents a model variable or approximation order, and the shown $\hat{h}$-curves illustrate how the truncated HAM solutions for the model depend on the convergence-control parameter $\hat{h}$. The main characteristic is the existence of a nearly horizontal (flat) region, approximately for $\hat{h} \in [-2, 0]$, where all curves cluster near zero. This indicates that the series solutions are convergent in this interval because they are stable and essentially insensitive to variations in $\hat{h}$. Outside this region, the curves diverge rapidly in both positive and negative directions, indicating numerical instability and loss of convergence. Consequently, the graph identifies the admissible range of $\hat{h}$ values that ensure reliable HAM solutions, with the flat portion of the curves representing the optimal choice, so we choose $\hat{h}$ as 1.

6 Results and discussions

Table 6.1 compares the numerical solutions for the susceptible population, $S(t)$, obtained using the ND Solver, RK4 method, and HAM. The results show that HAM achieves significantly smaller absolute errors than RK4, indicating higher accuracy. This is further supported by Figure 6.1, where the HAM solution closely overlaps with the ND Solver solution, while the RK4 solution shows slight deviations. Moreover, Figure 6.2 demonstrates that the absolute errors associated with HAM are nearly negligible compared to those of RK4, confirming the superior accuracy, efficiency, and reliability of HAM.

Table 6.1: ND Solve, RK4 and HAM solutions of susceptible human population $S(t)$ and their Absolute Errors (AE).

t	ND Solve	RK4	HAM	AE of RK4	AE of HAM
0	60.	60.	60.	0.	0.
0.1	59.921898	59.922176	59.921898	2.771×10^{-4}	1.231×10^{-9}
0.2	59.842859	59.843933	59.842859	1.073×10^{-3}	1.864×10^{-8}
0.3	59.762925	59.765261	59.762925	2.335×10^{-3}	8.301×10^{-9}
0.4	59.682140	59.686152	59.682140	4.011×10^{-3}	1.261×10^{-8}
0.5	59.600550	59.606596	59.600550	6.045×10^{-3}	2.473×10^{-8}
0.6	59.518202	59.526581	59.518203	8.378×10^{-3}	2.635×10^{-8}
0.7	59.435146	59.446098	59.435146	1.095×10^{-2}	2.801×10^{-8}
0.8	59.351430	59.365137	59.351430	1.370×10^{-2}	2.974×10^{-8}
0.9	59.267107	59.283686	59.267107	1.657×10^{-2}	3.088×10^{-8}
1.0	59.182228	59.201735	59.182229	1.950×10^{-2}	3.224×10^{-8}

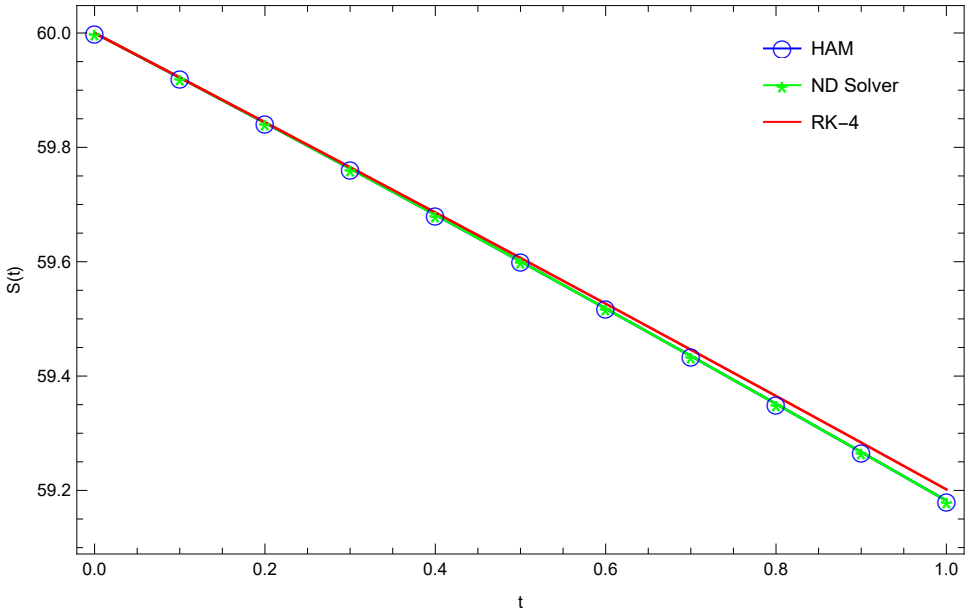

Figure 6.1: Geometrical interpretation of the ND Solver and HAM solutions for susceptible human population $S(t)$.

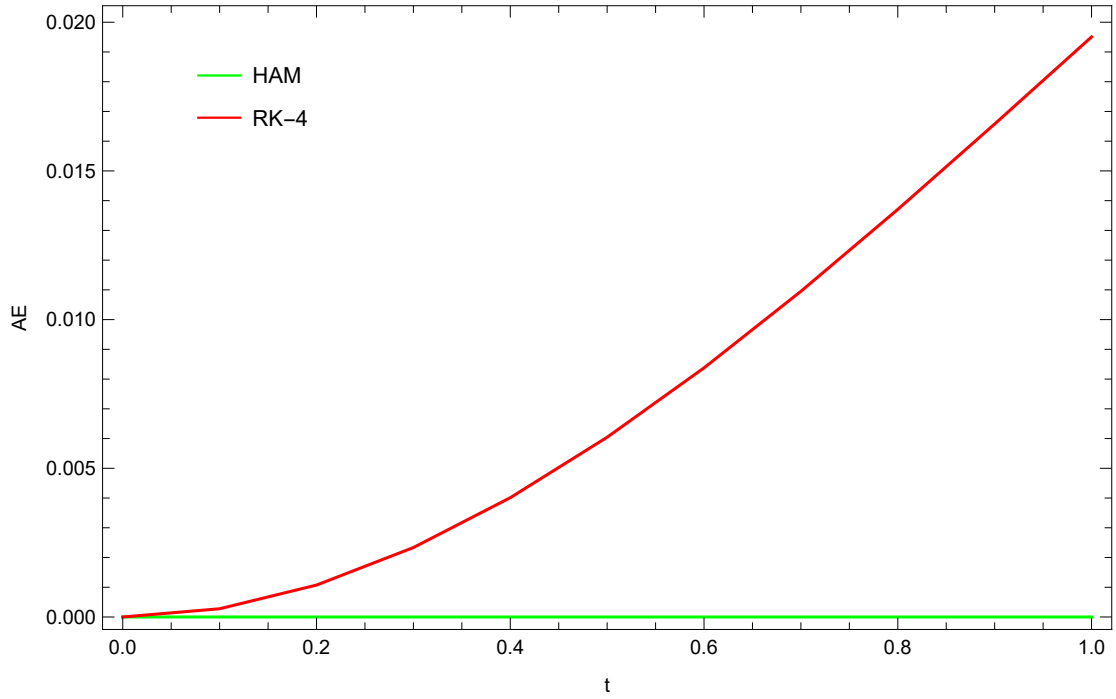

Figure 6.2: Error analysis of HAM and RK4 solutions with ND Solve solutions for susceptible population $S(t)$.

Table 6.2 presents the HAM solutions for the susceptible human population, $S(t)$, corresponding to different fractional orders α. The results show that the fractional-order parameter has a significant impact on the population dynamics, with $S(t)$ generally increasing as α approaches 1, indicating convergence toward the classical integer-order model. This behavior is illustrated in Figure 6.3, where lower values of α produce a faster initial decline in the susceptible population, while higher fractional orders yield trajectories that more closely resemble the integer-order system.

Table 6.2: HAM solutions of susceptible population $S(t)$ for different fractional values of α.

t	**HAM solutions**				
	$\alpha = 0.2$	$\alpha = 0.4$	$\alpha = 0.6$	$\alpha = 0.8$	$\alpha = 1$
0	60.	60.	60.	60.	60.
0.1	59.43625972	59.63759121	59.77658337	59.8662545	59.92189889
0.2	59.35047236	59.51743279	59.65779341	59.76511357	59.84285981
0.3	59.29479157	59.42937978	59.56020489	59.67273183	59.76292562
0.4	59.25270215	59.35745207	59.47420783	59.58539073	59.68214067
0.5	59.21854562	59.29565871	59.39594498	59.50151642	59.60055072
0.6	59.1896492	59.2409893	59.32339234	59.42026432	59.51820302
0.7	59.16452222	59.19168149	59.25532728	59.34112195	59.43514622
0.8	59.14224225	59.14659978	59.19094279	59.26375423	59.35143042
0.9	59.122196	59.10496236	59.12967244	59.18793108	59.26710709
1.0	59.10395358	59.06620405	59.07110026	59.11348921	59.18222912

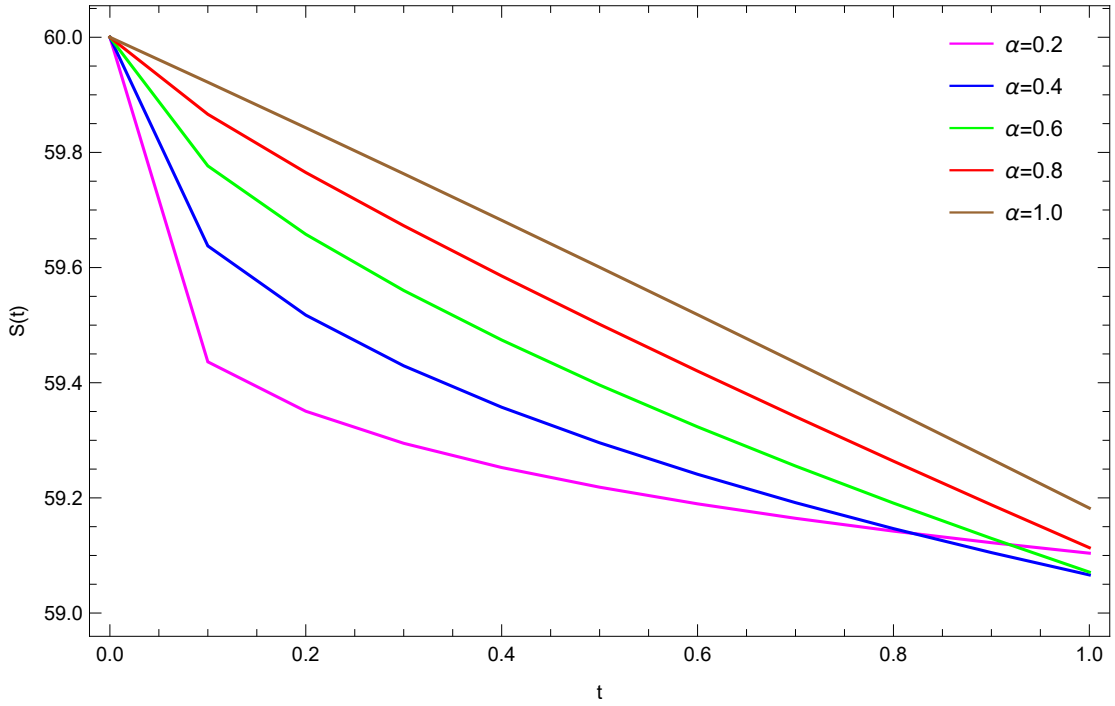

Figure 6.3: Graphical representation of HAM solutions of susceptible human population $S(t)$ for different fractional values of α.

Table 6.3: ND Solve, RK4 and HAM solutions of infected human population $I(t)$ and their Absolute Errors.

t	ND Solve	RK4	HAM	AE of RK4	AE of HAM
0	2.	2.	2.	0.	0.
0.1	2.077911	2.059498	2.077911	1.841×10^{-2}	1.472×10^{-9}
0.2	2.156373	2.120790	2.156373	3.558×10^{-2}	1.955×10^{-8}
0.3	2.235345	2.183928	2.235345	5.141×10^{-2}	1.068×10^{-8}
0.4	2.314783	2.248963	2.314783	6.582×10^{-2}	1.461×10^{-8}
0.5	2.394643	2.315951	2.394643	7.869×10^{-2}	2.528×10^{-8}
0.6	2.4748797	2.384945	2.474879	8.993×10^{-2}	2.686×10^{-8}
0.7	2.555446	2.456002	2.555446	9.944×10^{-2}	2.849×10^{-8}
0.8	2.636295	2.529181	2.636295	1.071×10^{-1}	3.016×10^{-8}
0.9	2.717377	2.604542	2.717377	1.128×10^{-1}	3.116×10^{-8}
1.0	2.798643	2.682144	2.798642	1.164×10^{-1}	3.236×10^{-8}

Table 6.3 compares the numerical solutions for the infected human population, $I(t)$, obtained using the ND Solver, RK4 method, and HAM. The results show that HAM yields significantly smaller absolute errors than RK4, demonstrating superior accuracy throughout the considered time interval. As illustrated in Figure 6.4, the HAM and ND Solver solution curves almost completely overlap, indicating excellent agreement, while Figure 6.5 confirms that the errors associated with HAM are nearly negligible compared to those of RK4. The numerical solutions also reveal an increasing trend in the infected population over time, which HAM accurately captures, highlighting its effectiveness and reliability in modeling system dynamics.

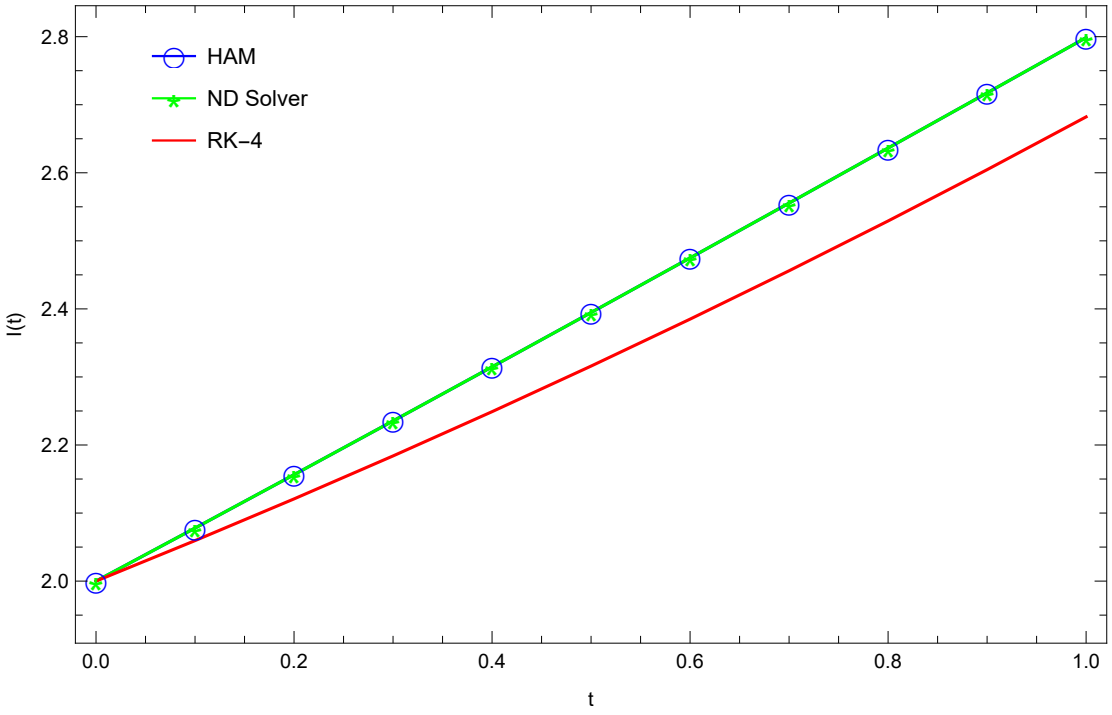

Figure 6.4: Geometrical interpretation of the ND Solver and HAM solutions for infected human population $I(t)$.

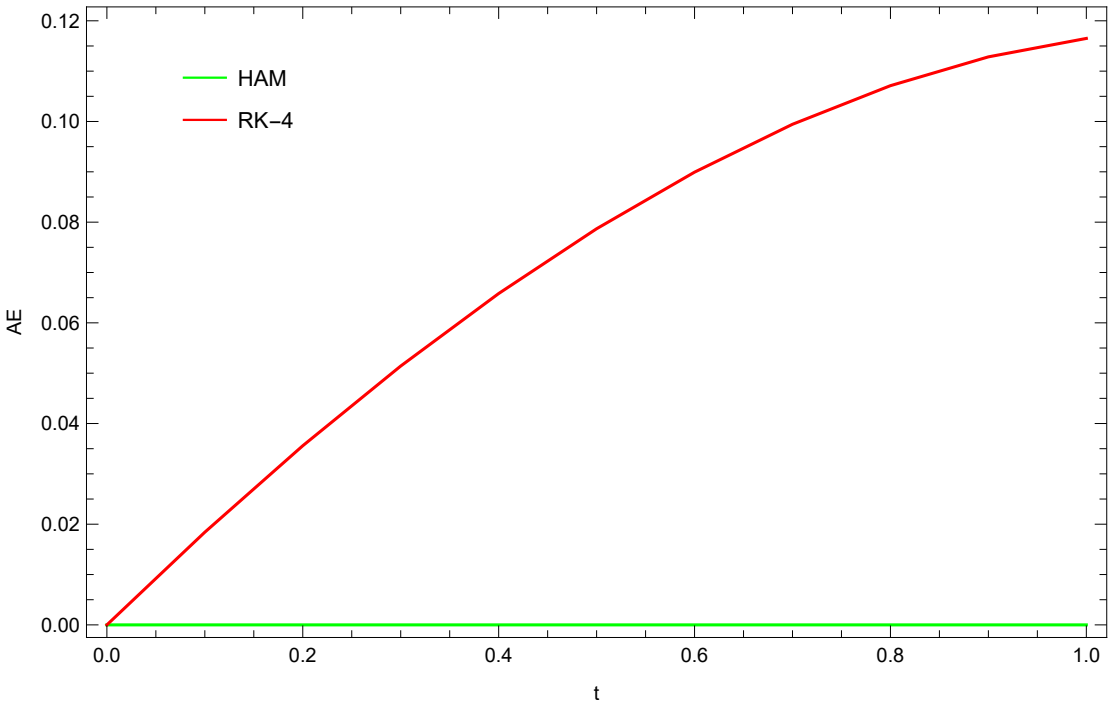

Figure 6.5: Error analysis of HAM and RK4 solutions with ND Solve solutions for infected human population $I(t)$.

Table 6.4: HAM solutions of infected population $I(t)$ for different fractional values of α.

t	**HAM solutions**				
	$\alpha = 0.2$	$\alpha = 0.4$	$\alpha = 0.6$	$\alpha = 0.8$	$\alpha = 1$
0	2.	2.	2.	2.	2.
0.1	2.546968342	2.355910496	2.221217146	2.133072167	2.077911468
0.2	2.627602268	2.471321075	2.337162276	2.232839619	2.156373791
0.3	2.679596885	2.555148827	2.431611098	2.323352951	2.235345317
0.4	2.718721672	2.623170145	2.514267542	2.408411823	2.314783128
0.5	2.750359034	2.681285864	2.58903778	2.489639762	2.394643057
0.6	2.777044489	2.732455736	2.657976677	2.56791661	2.474879698
0.7	2.800189056	2.778409766	2.722328466	2.643781928	2.555446423
0.8	2.820664284	2.820261108	2.782916329	2.717592749	2.6362954
0.9	2.839048718	2.858775221	2.840319366	2.789597623	2.717377604
1.0	2.855747283	2.894504836	2.894963817	2.85997581	2.798642842

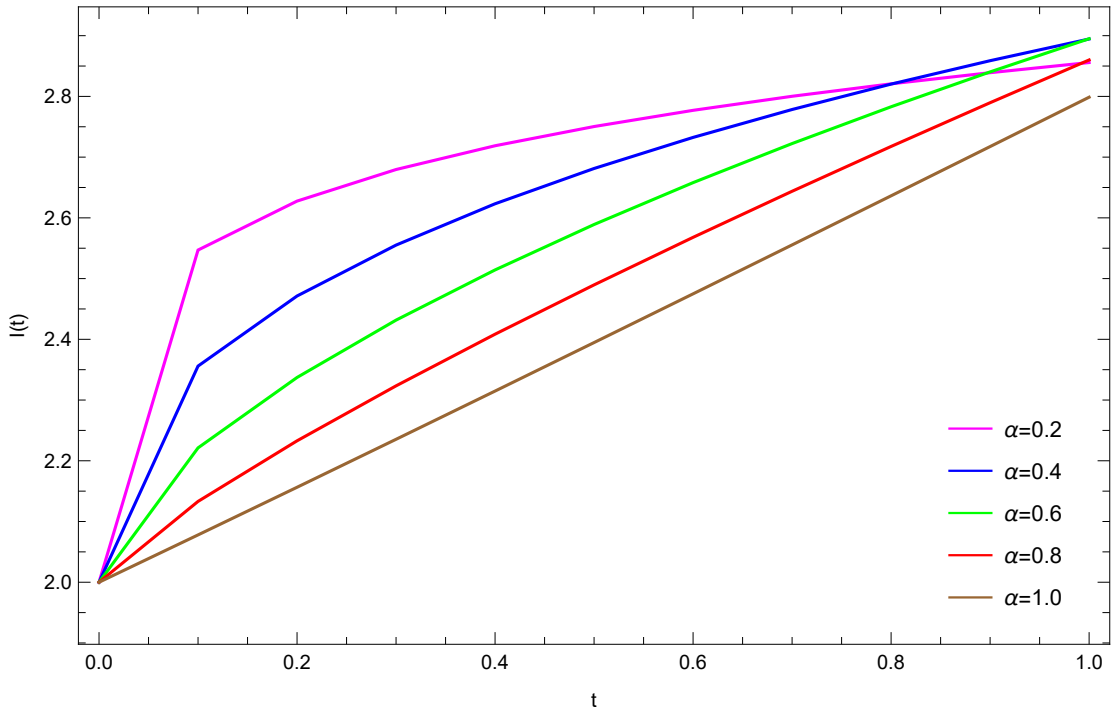

Figure 6.6: Graphical representation of HAM solutions of infected human population $I(t)$ for different fractional values of α.

Table 6.4 presents the HAM solutions for the infected human population, $I(t)$, corresponding to different fractional orders α. The results show that the fractional-order parameter significantly influences the infection dynamics, with smaller values of α leading to a more rapid initial increase in the infected population due to stronger memory effects. Figure 6.6 illustrates these trajectories, highlighting the distinct growth patterns associated with different fractional orders. As α approaches 1, the solutions gradually converge toward the behavior of the classical integer-order model, demonstrating the transition from fractional to classical dynamics.

Table 6.5: ND Solve, RK4 and HAM solutions of recovered human population $R(t)$ and their Absolute Errors.

t	ND Solve	RK4	HAM	AE of RK4	AE of HAM
0	1.	1.	1.	0.	0.
0.1	1.000189	1.000143	1.000189	4.664×10^{-5}	2.408×10^{-10}
0.2	1.000766	1.000586	1.000766	1.804×10^{-4}	9.116×10^{-10}
0.3	1.001729	1.001333	1.001729	3.960×10^{-4}	2.385×10^{-9}
0.4	1.003076	1.002392	1.003076	6.842×10^{-4}	2.003×10^{-9}
0.5	1.004806	1.003768	1.004806	1.038×10^{-3}	5.488×10^{-10}
0.6	1.006917	1.005470	1.006917	1.447×10^{-3}	5.143×10^{-10}
0.7	1.009407	1.007502	1.009407	1.905×10^{-3}	4.760×10^{-10}
0.8	1.012274	1.009873	1.012274	2.401×10^{-3}	4.238×10^{-10}
0.9	1.015515	1.012590	1.015515	2.920×10^{-3}	2.742×10^{-10}
1.0	1.019128	1.015661	1.019128	3.467×10^{-3}	1.280×10^{-10}

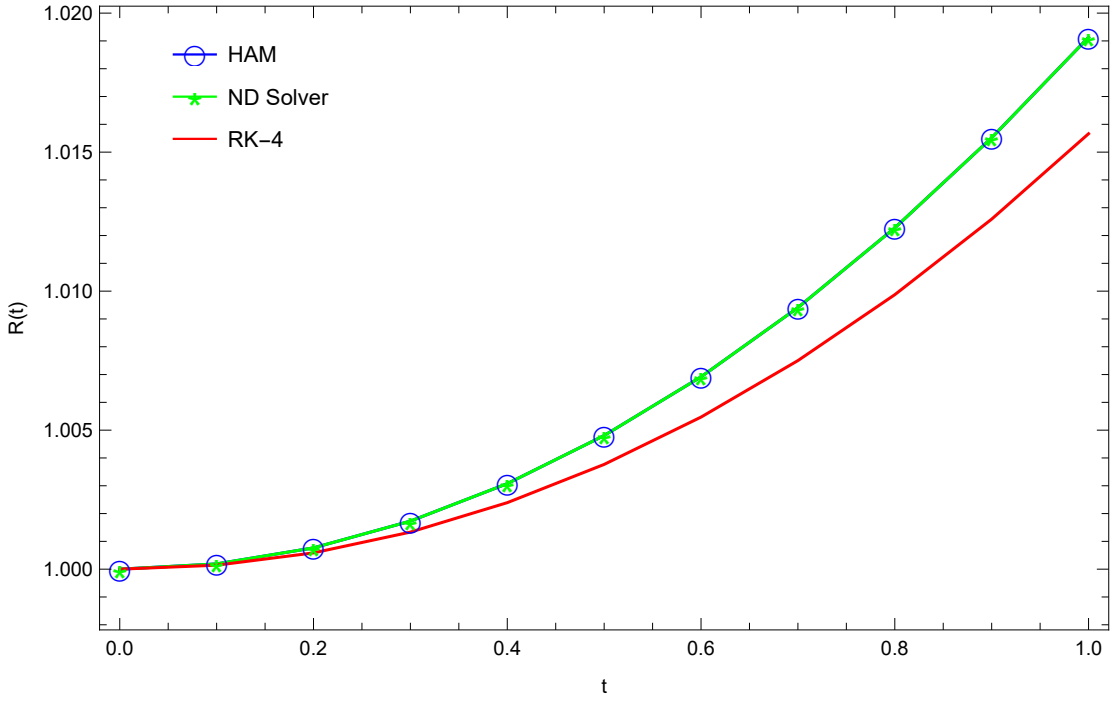

Figure 6.7: Geometrical interpretation of the ND Solver and HAM solutions for recovered human population $R(t)$.

Table 6.5 compares the numerical solutions for the recovered human population, $R(t)$, obtained using the ND Solver, RK4 method, and HAM. The results show that HAM achieves remarkably high accuracy, with absolute errors smaller than those of RK4. As illustrated in Figure 6.7, the HAM and ND Solver solution curves exhibit an almost perfect overlap, confirming the reliability of HAM. Moreover, Figure 6.8 shows that the RK4 error increases over time, whereas the HAM error remains nearly negligible throughout the simulation interval, highlighting the superior accuracy and stability of HAM in modeling the recovered population dynamics.

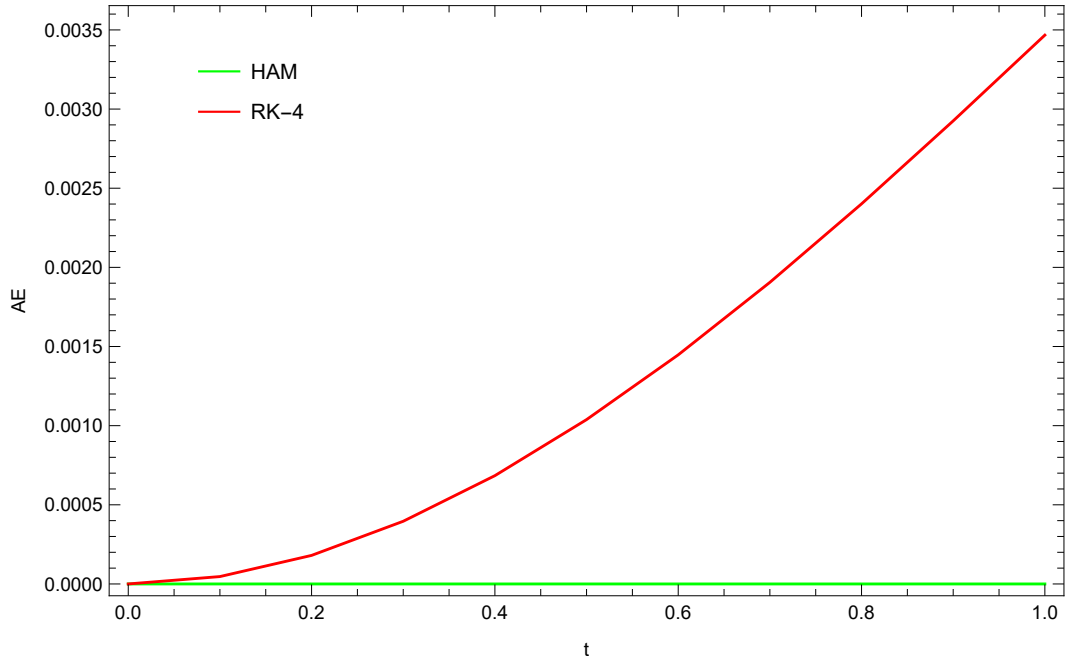

Figure 6.8: Error analysis of HAM and RK4 solutions with ND Solve solutions for recovered human population $R(t)$.

Table 6.6: HAM solutions of recovered human population $R(t)$ for different fractional values of α.

t	**HAM solutions**				
	$\alpha = 0.2$	$\alpha = 0.4$	$\alpha = 0.6$	$\alpha = 0.8$	$\alpha = 1$
0	1.	1.	1.	1.	1.
0.1	1.016771933	1.006498299	1.002199486	1.000673335	1.000189642
0.2	1.021925375	1.011246135	1.005044312	1.002046813	1.0007664
0.3	1.025611541	1.015471394	1.008184014	1.003915221	1.00172906
0.4	1.028576182	1.019377784	1.011524628	1.006197451	1.003076206
0.5	1.031095345	1.023055423	1.015017241	1.008843814	1.004806221
0.6	1.033306314	1.026554966	1.018630988	1.011819071	1.006917281
0.7	1.035288726	1.029908744	1.022344258	1.015096126	1.009407352
0.8	1.037093463	1.033139114	1.026140883	1.018653022	1.012274185
0.9	1.038755287	1.036262421	1.030008194	1.022471293	1.015515311
1.0	1.040299142	1.039291117	1.033935918	1.026534978	1.019128041

Table 6.6 presents the HAM solutions for the recovered human population, $R(t)$, corresponding to different fractional orders α. The results indicate that the fractional-order parameter significantly affects the recovery dynamics, with lower values of α producing a faster initial increase in the recovered population, while higher values lead to behavior that gradually approaches the classical integer-order model. This trend is illustrated in Figure 6.9 through the distinct trajectories of $R(t)$ for the selected fractional orders. Overall, the findings demonstrate that the Homotopy Analysis Method is a reliable and efficient approach for analyzing and simulating the transmission dynamics of Listeria infection under varying environmental conditions.

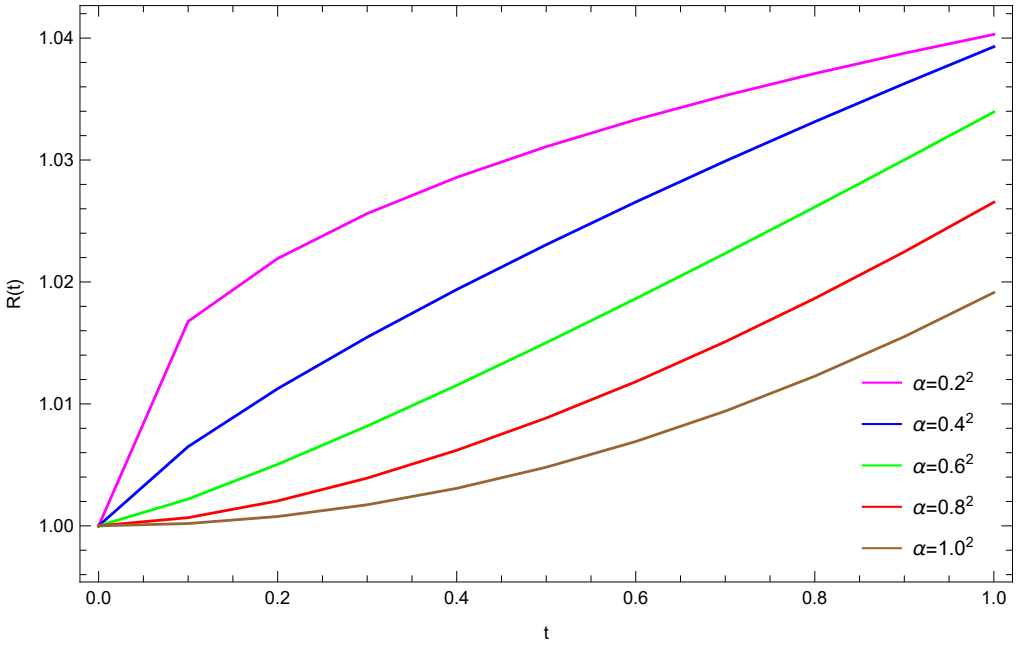

Figure 6.9: Graphical representation of HAM solutions of recovered human population $R(t)$ for different fractional values of α.

Table 6.7: ND Solve, RK4 and HAM solutions of Listeria bacteria population $L_c(t)$ and their Absolute Errors.

t	ND Solve	RK4	HAM	AE of RK4	AE of HAM
0	0.460517	0.460517	0.460517	0.	0.
0.1	0.439504	0.439603	0.439504	9.808×10^{-5}	1.950×10^{-9}
0.2	0.417648	0.418032	0.417648	3.836×10^{-4}	9.446×10^{-9}
0.3	0.394940	0.395784	0.394940	8.431×10^{-4}	1.277×10^{-8}
0.4	0.371376	0.372839	0.371376	1.462×10^{-3}	1.210×10^{-8}
0.5	0.346949	0.349176	0.346949	2.226×10^{-3}	9.039×10^{-9}
0.6	0.321655	0.324773	0.321655	3.117×10^{-3}	9.115×10^{-9}
0.7	0.295488	0.299609	0.295488	4.120×10^{-3}	9.189×10^{-9}
0.8	0.268445	0.273660	0.268445	5.214×10^{-3}	9.229×10^{-9}
0.9	0.240523	0.246902	0.240523	6.378×10^{-3}	8.911×10^{-9}
1.0	0.211718	0.219313	0.211718	7.594×10^{-3}	8.623×10^{-9}

Table 6.7 compares the numerical solutions for the environmental Listeria bacterial population, $L_c(t)$, obtained using the ND Solver, RK4 method, and HAM. The results show that HAM achieves significantly higher accuracy and smaller absolute errors, whereas RK4 exhibits comparatively larger errors. As illustrated in Figure 6.10, the HAM and ND Solver solution curves nearly coincide, demonstrating excellent agreement and confirming the reliability of HAM. Furthermore, Figure 6.11 shows that the absolute error associated with HAM remains almost negligible throughout the simulation period, whereas the RK4 error increases with time, highlighting the superior accuracy and stability of HAM in modeling the environmental Listeria bacterial population dynamics.

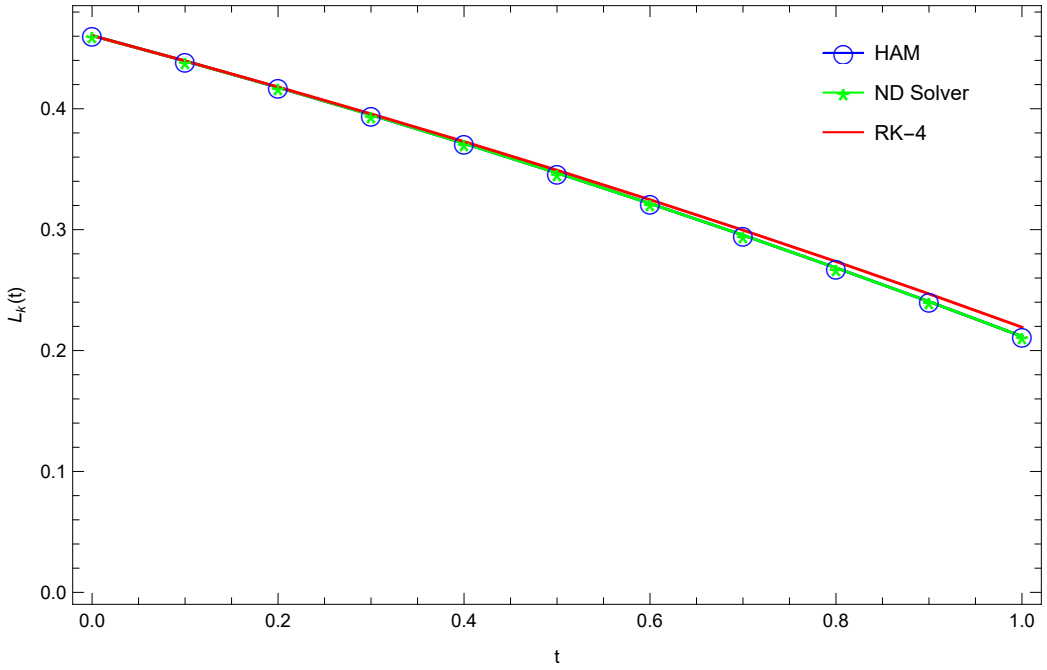

Figure 6.10: Geometrical interpretation of the ND Solver and HAM solutions for Listeria bacteria population $L_c(t)$.

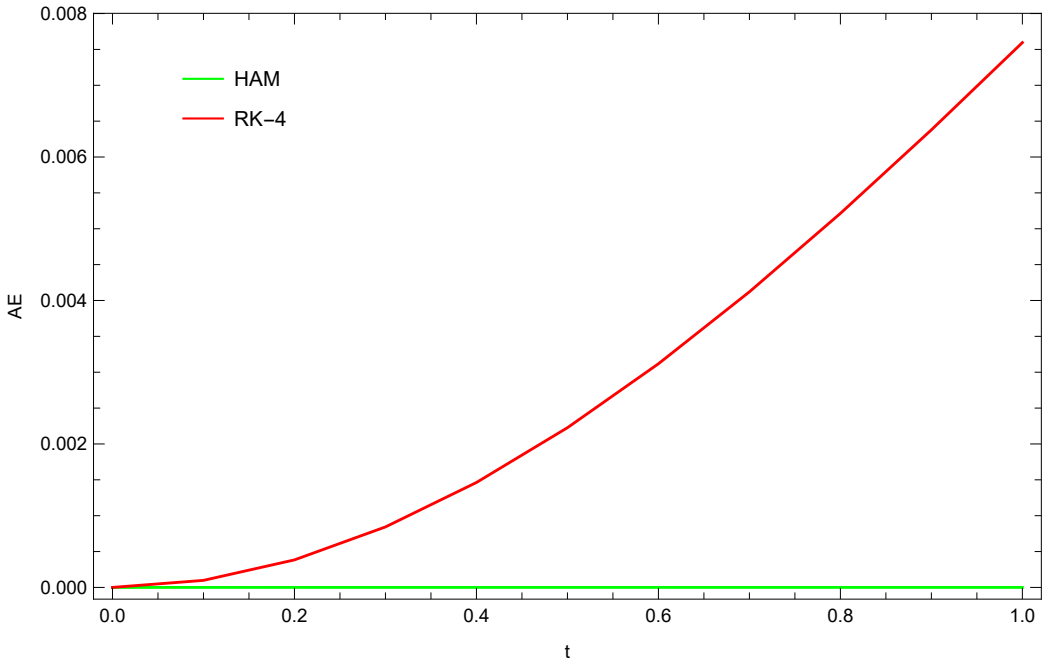

Figure 6.11: Error analysis of HAM and RK4 solutions with ND Solve solutions for Listeria bacteria population $L_c(t)$.

Table 6.8 presents the HAM solutions for the environmental Listeria bacterial population, $L_c(t)$, corresponding to different fractional orders α. The results show that the fractional-order parameter significantly influences the bacterial dynamics, with smaller values of α leading to a more rapid decline in the bacterial population compared to the classical integer-order case

($\alpha = 1$). As illustrated in Figure 6.12, the decay trajectories of $L_c(t)$ vary distinctly with α, demonstrating that lower fractional orders accelerate the reduction of bacterial concentration, while higher values gradually approach the behavior of the integer-order model.

Table 6.8: HAM solutions of Listeria bacteria population $L_c(t)$ for different fractional values of α.

t	**HAM solutions**				
	$\alpha = 0.2$	$\alpha = 0.4$	$\alpha = 0.6$	$\alpha = 0.8$	$\alpha = 1$
0	0.4605170186	0.4605170186	0.4605170186	0.4605170186	0.4605170186
0.1	0.2802547523	0.3535405465	0.3977694735	0.4239954549	0.4395049088
0.2	0.2468195365	0.3130945788	0.3615502274	0.3949993473	0.4176483094
0.3	0.2241158612	0.2817651939	0.3302779209	0.3674752742	0.394940792
0.4	0.2063975638	0.2550589427	0.3015583323	0.3405349397	0.3713763677
0.5	0.1916492807	0.2312783783	0.2744509948	0.3138162502	0.3469494996
0.6	0.1789029111	0.2095660241	0.2484722738	0.2871314388	0.3216551175
0.7	0.1676111741	0.1894178499	0.223335796	0.2603703681	0.2954886304
0.8	0.1574314901	0.1705080249	0.1988563311	0.2334635318	0.2684459401
0.9	0.1481337804	0.1526115985	0.1749065621	0.2063650367	0.2405234547
1.0	0.139555322	0.1355655712	0.1513950115	0.1790437704	0.2117181008

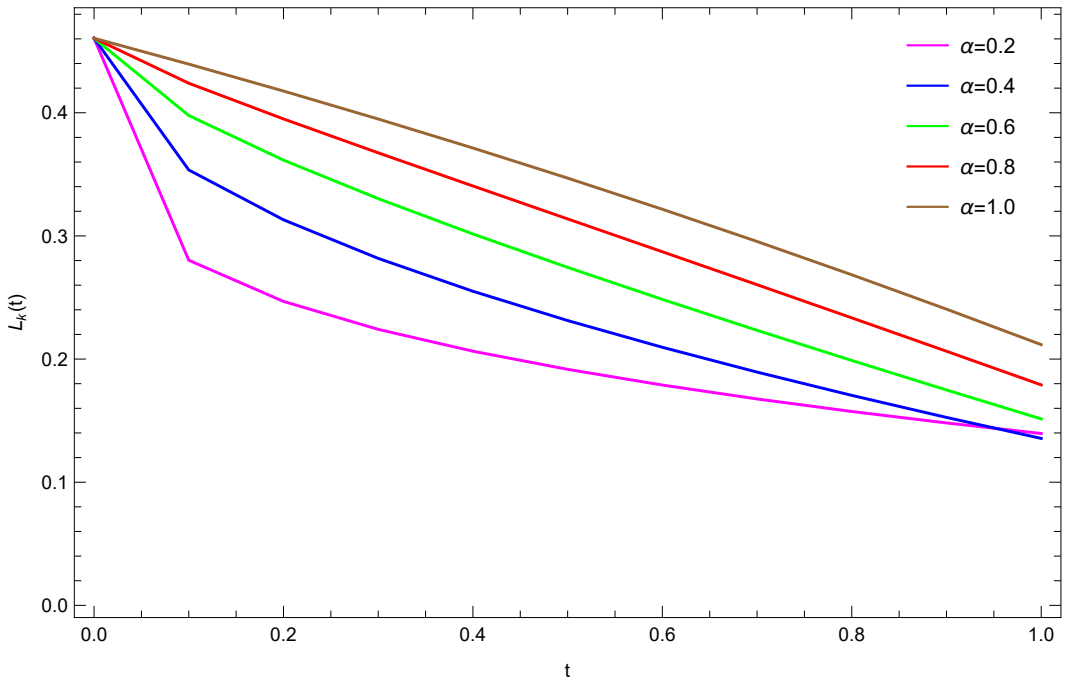

Figure 6.12: Graphical representation of HAM solutions of Listeria bacteria population $L_c(t)$ for different fractional values of α.

Table 6.9: ND Solve, RK4 and HAM solutions of contaminated food $F_c(t)$ and their Absolute Errors.

t	ND Solve	RK4	HAM	AE of RK4	AE of HAM
0	30.	30.	30.	0.	0.
0.1	29.971028	29.970971	29.971028	5.798×10^{-5}	7.901×10^{-11}
0.2	29.942115	29.942000	29.942115	1.158×10^{-4}	1.568×10^{-10}
0.3	29.913260	29.913087	29.913260	1.734×10^{-4}	1.583×10^{-10}
0.4	29.884462	29.884232	29.884462	2.307×10^{-4}	1.575×10^{-10}
0.5	29.855722	29.855435	29.855722	2.875×10^{-4}	1.554×10^{-10}
0.6	29.827039	29.826695	29.827039	3.448×10^{-4}	1.551×10^{-10}
0.7	29.798414	29.798013	29.798414	4.013×10^{-4}	1.548×10^{-10}
0.8	29.769846	29.769389	29.769846	4.571×10^{-4}	1.545×10^{-10}
0.9	29.741334	29.740821	29.741334	5.139×10^{-4}	1.542×10^{-10}
1.0	29.712880	29.712311	29.712880	5.697×10^{-4}	1.539×10^{-10}

Table 6.9 compares the numerical solutions for the contaminated food compartment, $F_c(t)$, obtained using the ND Solver, RK4 method, and HAM. The results indicate that HAM achieves exceptionally high accuracy, with absolute errors of the smaller order, whereas RK4 produces comparatively larger errors throughout the simulation period. As shown in Figure 6.13, the HAM and ND Solver solution curves exhibit an almost perfect overlap, confirming the excellent agreement and reliability of HAM. Furthermore, Figure 6.14 demonstrates that the error associated with HAM remains virtually negligible over the entire time interval, while the RK4 error increases progressively with time, highlighting the superior accuracy, convergence, and stability of HAM in modeling the dynamics of the contaminated food compartment, $F_c(t)$.

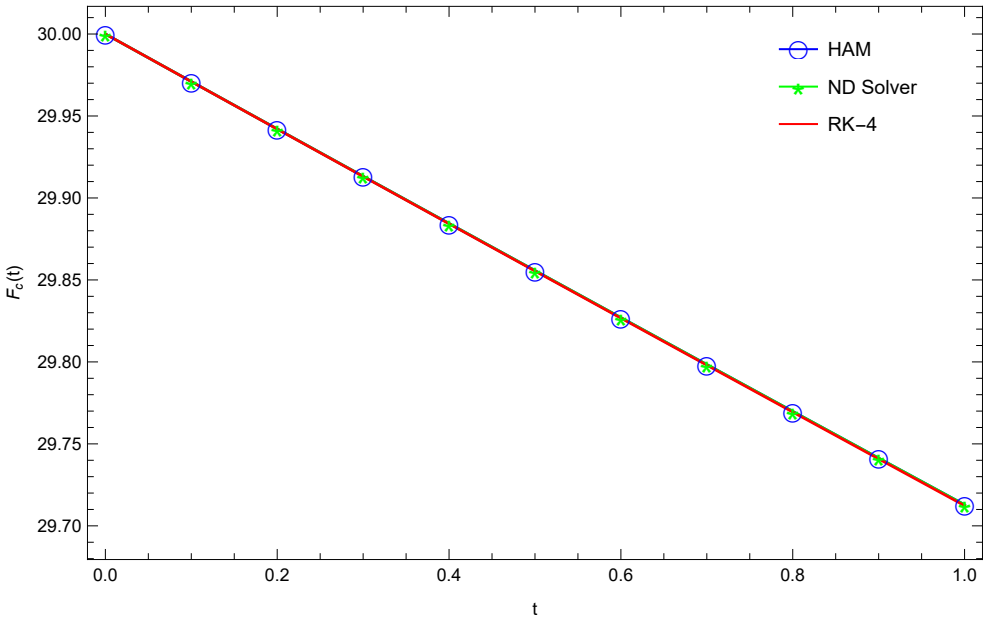

Figure 6.13: Geometrical interpretation of the ND Solver and HAM solutions for contaminated food $F_c(t)$.

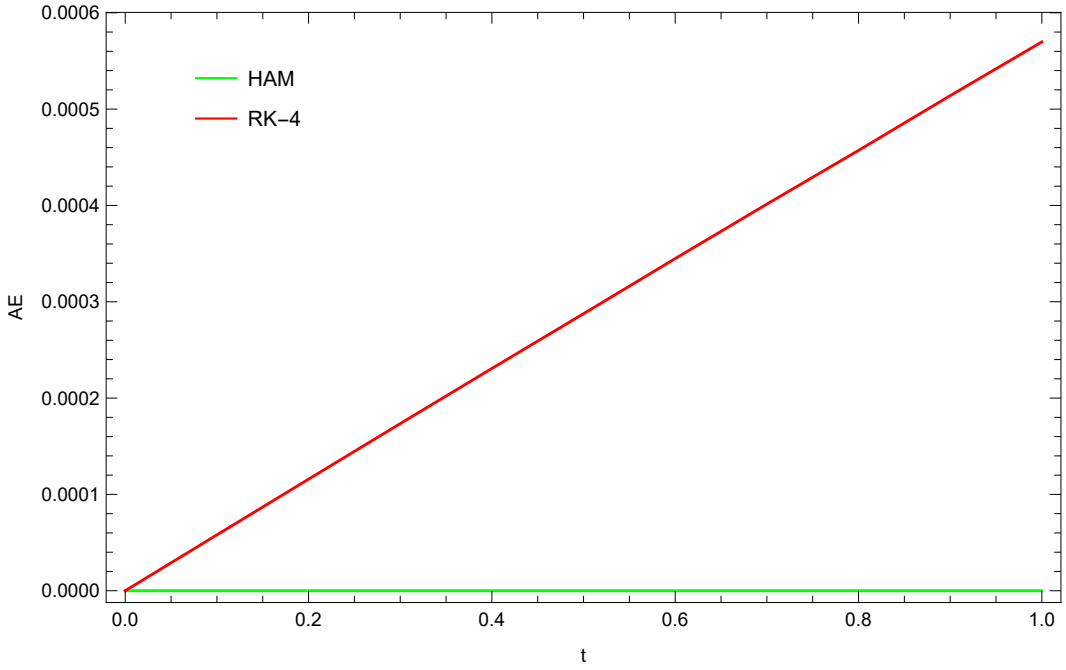

Figure 6.14: Error analysis of HAM and RK4 solutions with ND Solve solutions for contaminated food $F_c(t)$.

Table 6.10: HAM solutions of contaminated food $F_c(t)$ for different fractional values of α.

t	**HAM solutions**				
	$\alpha = 0.2$	$\alpha = 0.4$	$\alpha = 0.6$	$\alpha = 0.8$	$\alpha = 1$
0	30.	30.	30.	30.	30.
0.1	29.80328478	29.87086001	29.91880508	29.95075378	29.97102898
0.2	29.77446633	29.83000843	29.877189	29.9143883	29.94211585
0.3	29.75572043	29.80042554	29.84362886	29.88174785	29.91326048
0.4	29.74149864	29.77640452	29.81444235	29.8513371	29.88446277
0.5	29.72990985	29.75582722	29.78814138	29.82249893	29.85572259
0.6	29.7200637	29.73763809	29.76394053	29.79486605	29.82703984
0.7	29.71146477	29.72122376	29.7413628	29.76820526	29.79841439
0.8	29.70380706	29.70619171	29.7200917	29.7423561	29.76984614
0.9	29.69688738	29.69227345	29.69990399	29.71720177	29.74133497
1.0	29.69056349	29.67927607	29.68063494	29.69265373	29.71288076

Table 6.10 presents the HAM solutions for the contaminated food compartment, $F_c(t)$, corresponding to different fractional orders α. The results show that the fractional-order parameter significantly influences the contamination dynamics, with smaller values of α yielding lower levels of contamination compared to the classical integer-order case $(\alpha = 1)$. As illustrated in Figure 6.15, the trajectories of $F_c(t)$ vary distinctly with the fractional order, where lower values of α lead to a more pronounced decline in contaminated food levels, while higher values gradually approach the behavior of the integer-order model. These findings emphasize the role of memory effects in contamination processes and highlight the importance of fractional-order modeling for accurately capturing their temporal evolution.

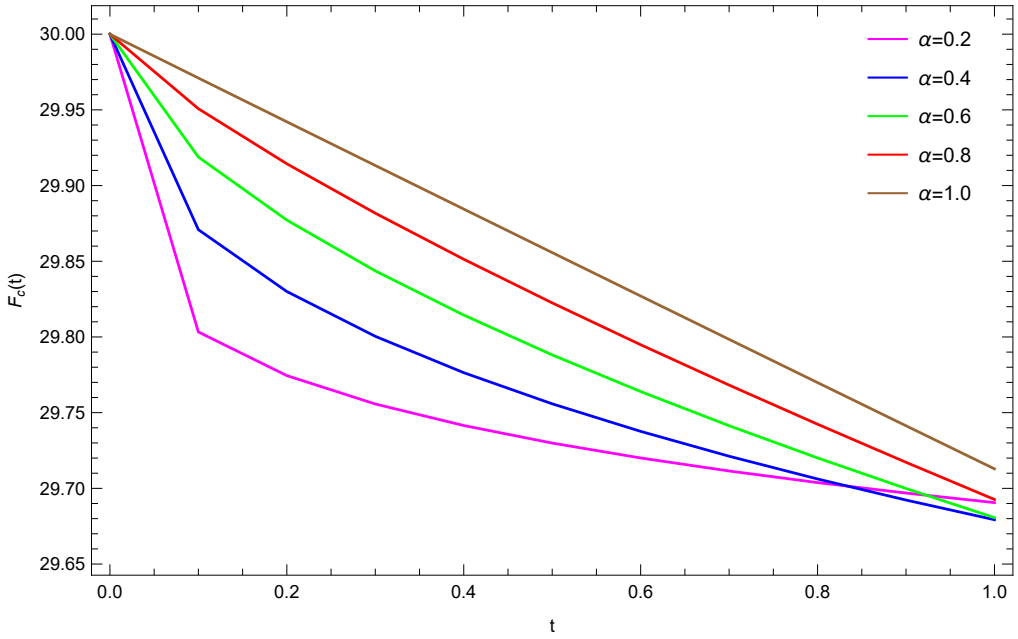

Figure 6.15: Graphical representation of HAM solutions of contaminated food $F_c(t)$ for different fractional values of α.

Table 6.11: ND Solve, RK4 and HAM solutions of uncontaminated food $F_u(t)$ and their Absolute Errors.

t	ND Solve	RK4	HAM	AE of RK4	AE of HAM
0	1.	1.	1.	0.	0.
0.1	1.028971	1.029029	1.028971	5.798×10^{-5}	7.902×10^{-11}
0.2	1.057884	1.058000	1.057884	1.158×10^{-4}	1.568×10^{-10}
0.3	1.086739	1.086913	1.086739	1.734×10^{-4}	1.583×10^{-10}
0.4	1.115537	1.115768	1.115537	2.307×10^{-4}	1.575×10^{-10}
0.5	1.144277	1.144565	1.144277	2.875×10^{-4}	1.554×10^{-10}
0.6	1.172960	1.173305	1.172960	3.448×10^{-4}	1.551×10^{-10}
0.7	1.201585	1.201987	1.201585	4.013×10^{-4}	1.548×10^{-10}
0.8	1.230153	1.230611	1.230153	4.571×10^{-4}	1.545×10^{-10}
0.9	1.258665	1.259179	1.258665	5.139×10^{-4}	1.542×10^{-10}
1.0	1.287119	1.287689	1.287119	5.697×10^{-4}	1.539×10^{-10}

Table 6.11 compares the numerical solutions for the uncontaminated food compartment, $F_u(t)$, obtained using the ND Solver, RK4 method, and HAM. As illustrated in Figure 6.16, the HAM and ND Solver solution curves almost perfectly overlap, confirming the excellent agreement and reliability of the HAM approach. Moreover, Figure 6.17 demonstrates that the error associated with RK4 increases over time, whereas the HAM error remains virtually negligible throughout the simulation period, highlighting the accuracy, convergence, and stability of HAM in modeling the dynamics of the uncontaminated food compartment, $F_u(t)$.

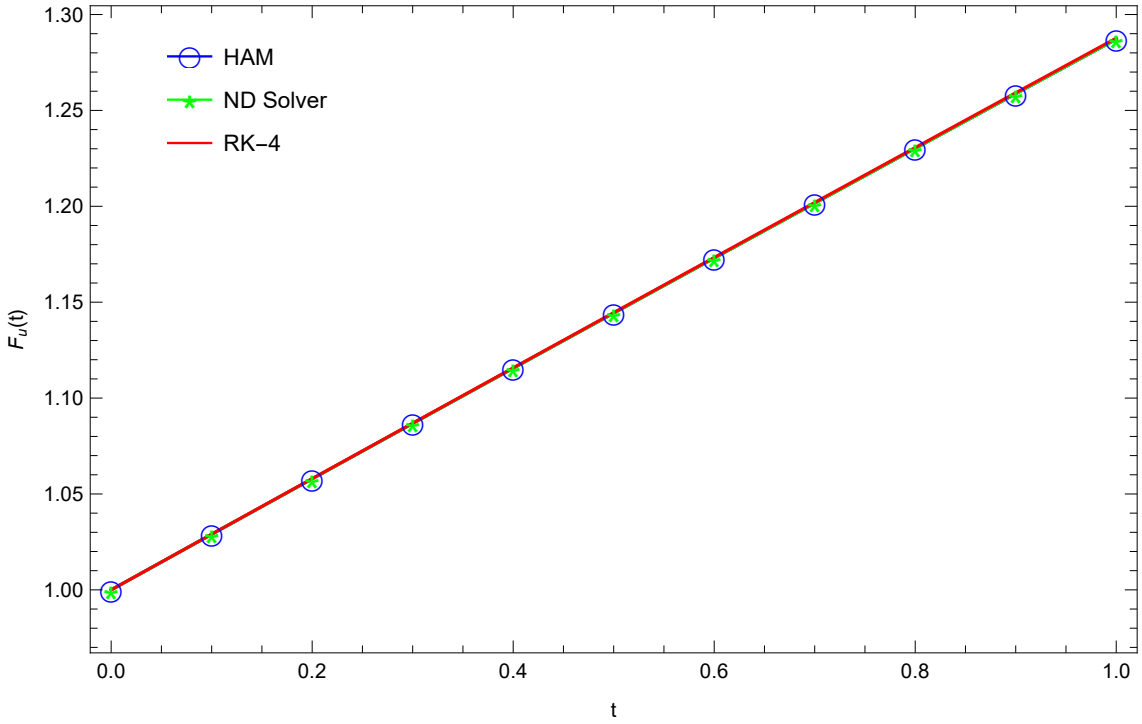

Figure 6.16: Geometrical interpretation of the ND Solver and HAM solutions for uncontaminated food $F_u(t)$.

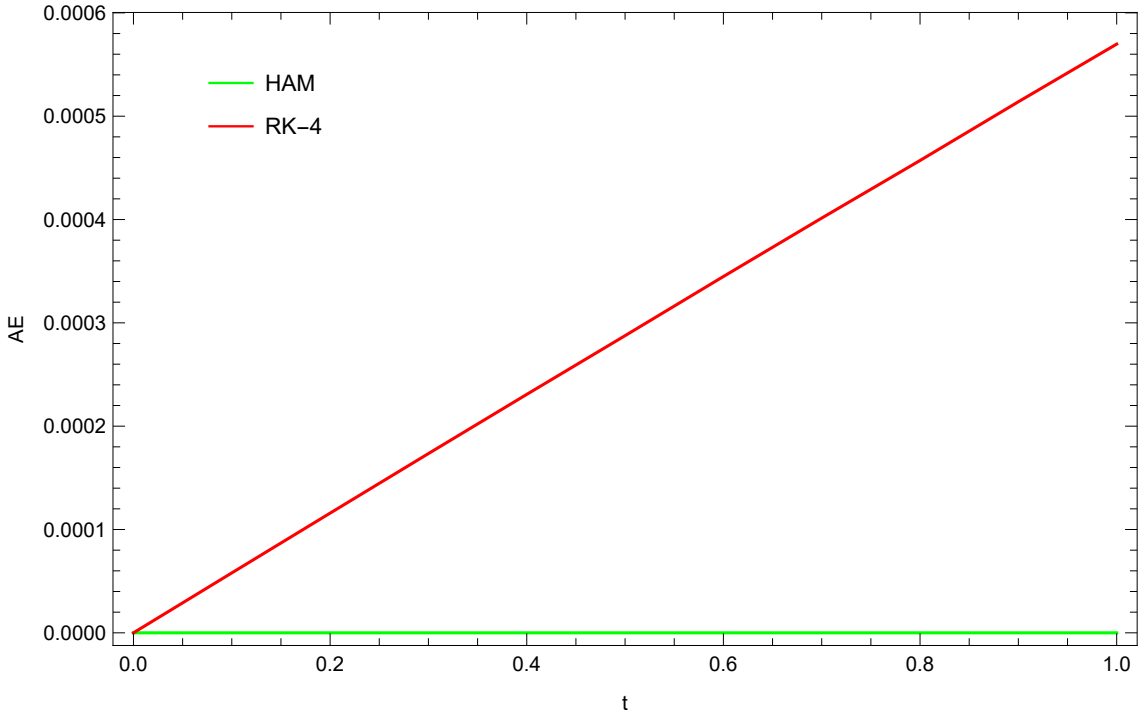

Figure 6.17: Error analysis of HAM and RK4 solutions with ND Solve solutions for uncontaminated food $F_u(t)$.

Table 6.12 presents the HAM solutions for the uncontaminated food compartment, $F_u(t)$,

corresponding to different fractional orders α. The results indicate that the fractional-order parameter has a significant effect on the dynamics of the uncontaminated food population, with $F_u(t)$ increasing over time from its initial level. As shown in Figure 6.18, lower fractional orders lead to a more rapid initial increase in the uncontaminated food compartment, while higher values of α produce dynamics that gradually converge to those of the integer-order model. These findings highlight the importance of fractional-order modeling in capturing memory effects and accurately describing the temporal evolution of food contamination and decontamination processes.

Table 6.12: HAM solutions of uncontaminated food $F_u(t)$ for different fractional values of α.

t	**HAM solutions**				
	$\alpha = 0.2$	$\alpha = 0.4$	$\alpha = 0.6$	$\alpha = 0.8$	$\alpha = 1$
0	1.	1.	1.	1.	1.
0.1	1.196715218	1.129139994	1.081194922	1.049246222	1.028971019
0.2	1.22553367	1.169991575	1.122811005	1.085611704	1.057884155
0.3	1.244279566	1.199574462	1.156371143	1.11825215	1.086739521
0.4	1.258501355	1.223595478	1.185557651	1.148662897	1.115537235
0.5	1.270090147	1.244172775	1.21185862	1.177501068	1.144277411
0.6	1.279936301	1.262361908	1.236059467	1.205133949	1.172960164
0.7	1.288535226	1.278776244	1.258637201	1.231794736	1.201585608
0.8	1.296192938	1.293808292	1.279908303	1.257643902	1.230153859
0.9	1.303112616	1.30772655	1.300096011	1.282798229	1.258665031
1.0	1.30943651	1.320723933	1.319365057	1.307346274	1.287119237

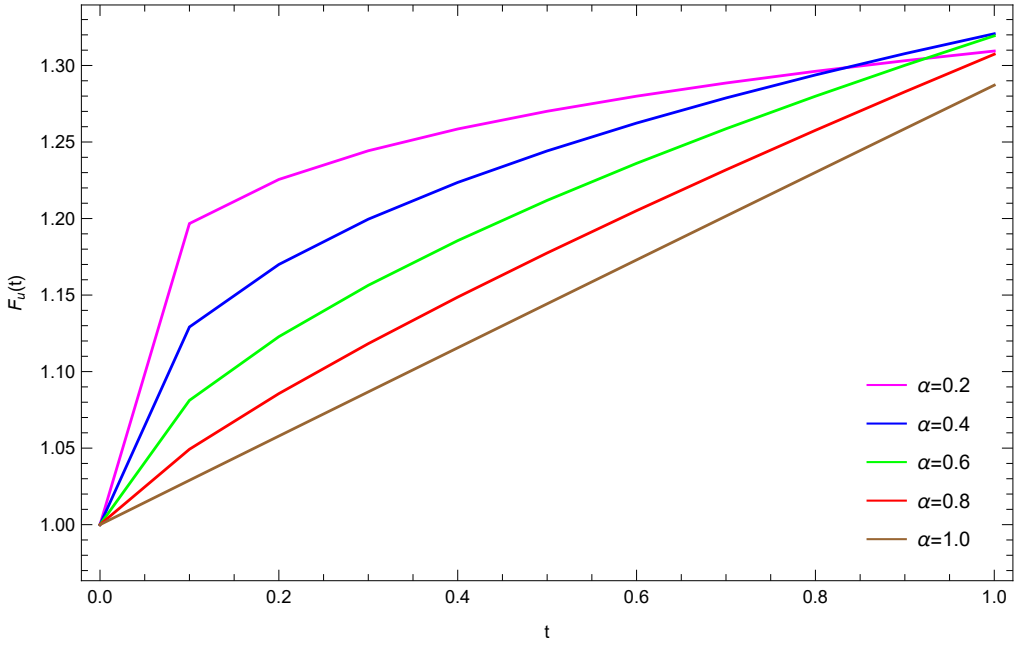

Figure 6.18: Graphical representation of HAM solutions of uncontaminated food $F_u(t)$ for different fractional values of α.

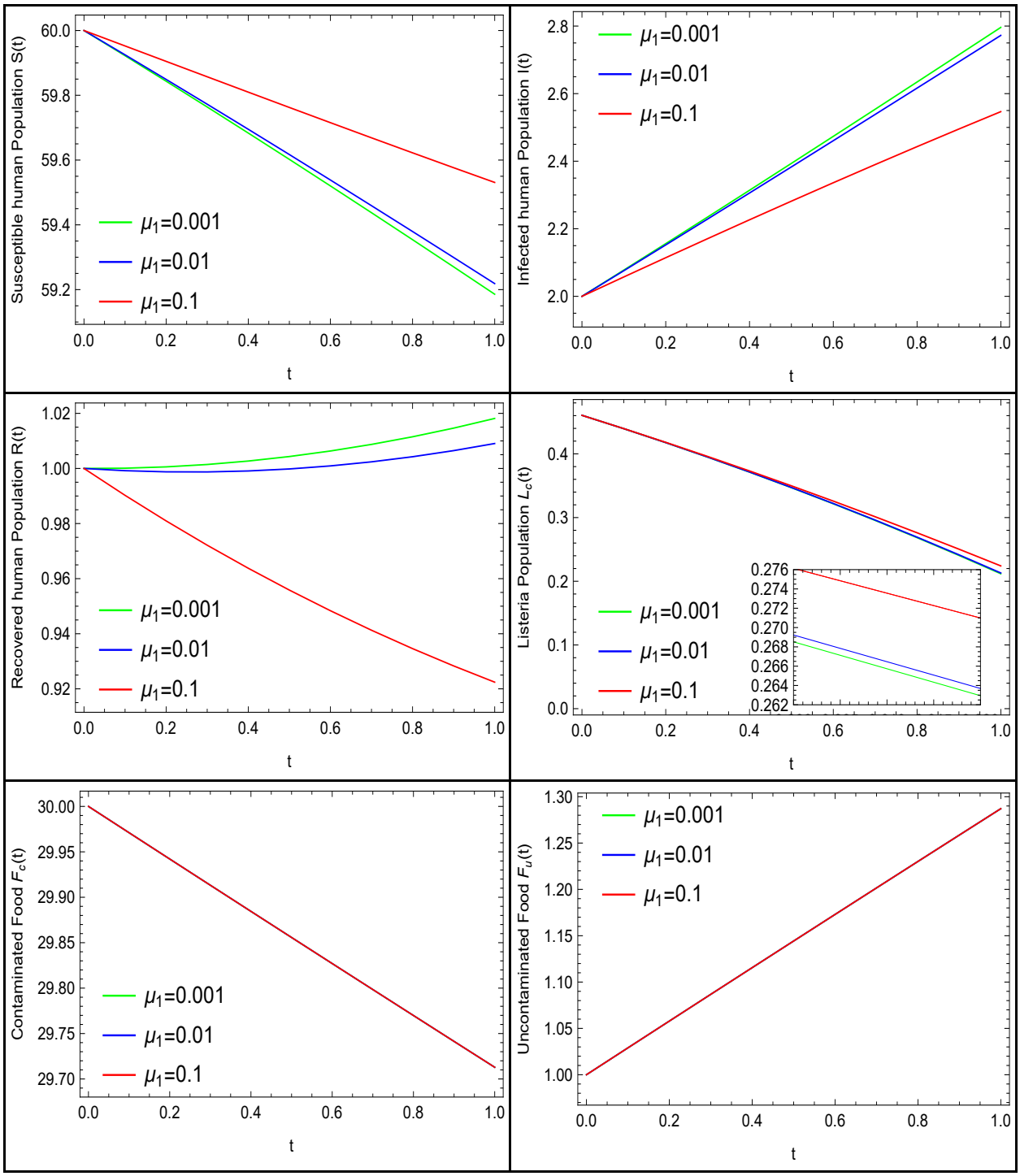

Figure 6.19: Nature of the model with the increase in μ_1, the mortality rate of each population class.

Figures 6.19–6.25 illustrate the sensitivity of the model to variations in key epidemiological and environmental parameters. Figure 6.19 examines the effect of the mortality rate, μ_1, and shows that an increase in mortality leads to a rise in the susceptible and environmental Listeria populations, while the infected and recovered populations decrease. The contaminated and

uncontaminated food compartments remain unaffected by changes in this parameter.

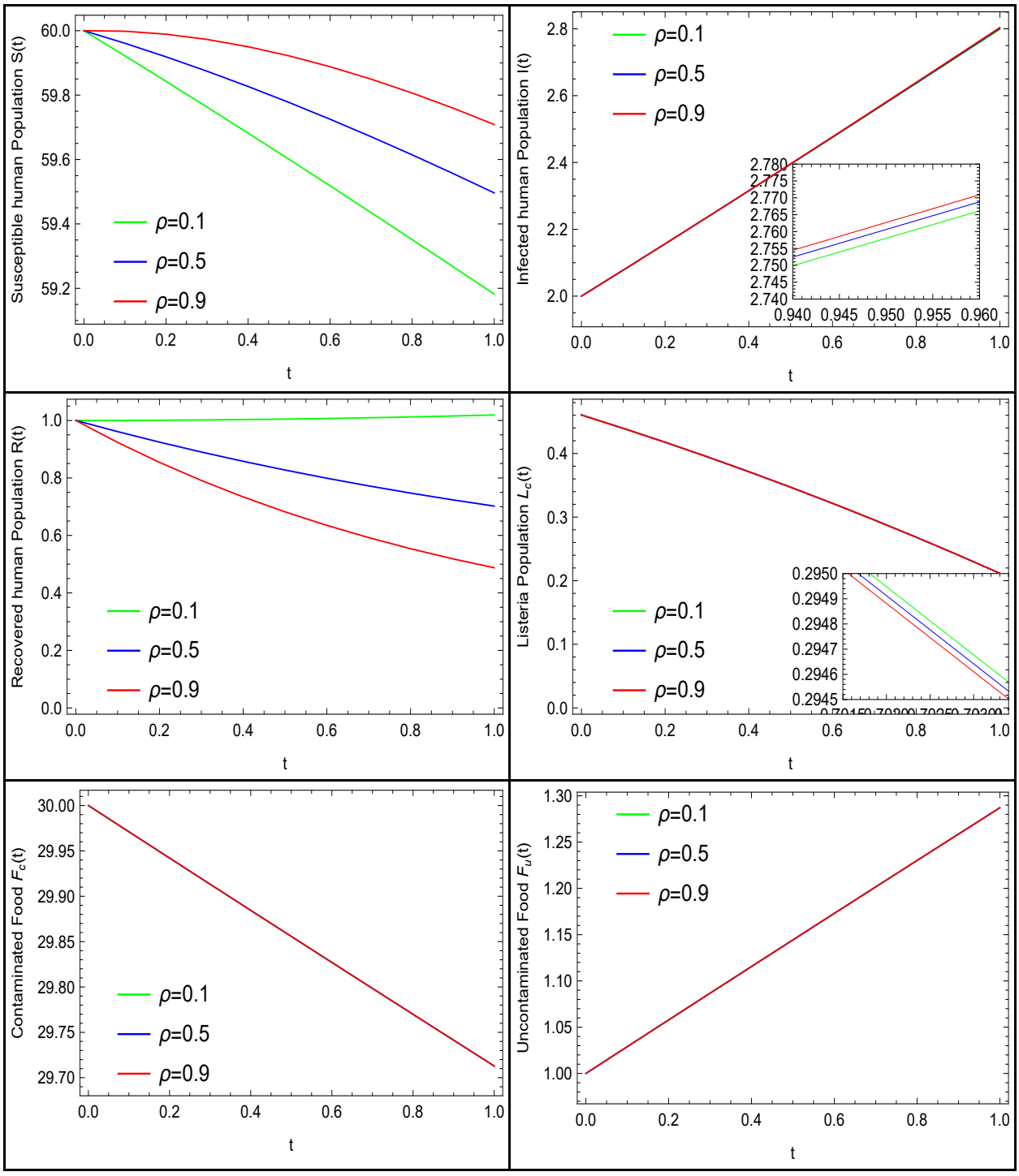

Figure 6.20: Nature of the model with the increase in ρ, the recovered rate.

Figure 6.20 depicts the influence of the immunity-loss rate, ρ. The results indicate that as ρ increases, both the susceptible and infected populations increase, whereas the recovered and environmental Listeria populations decline. No noticeable changes are observed in the

food-related compartments.

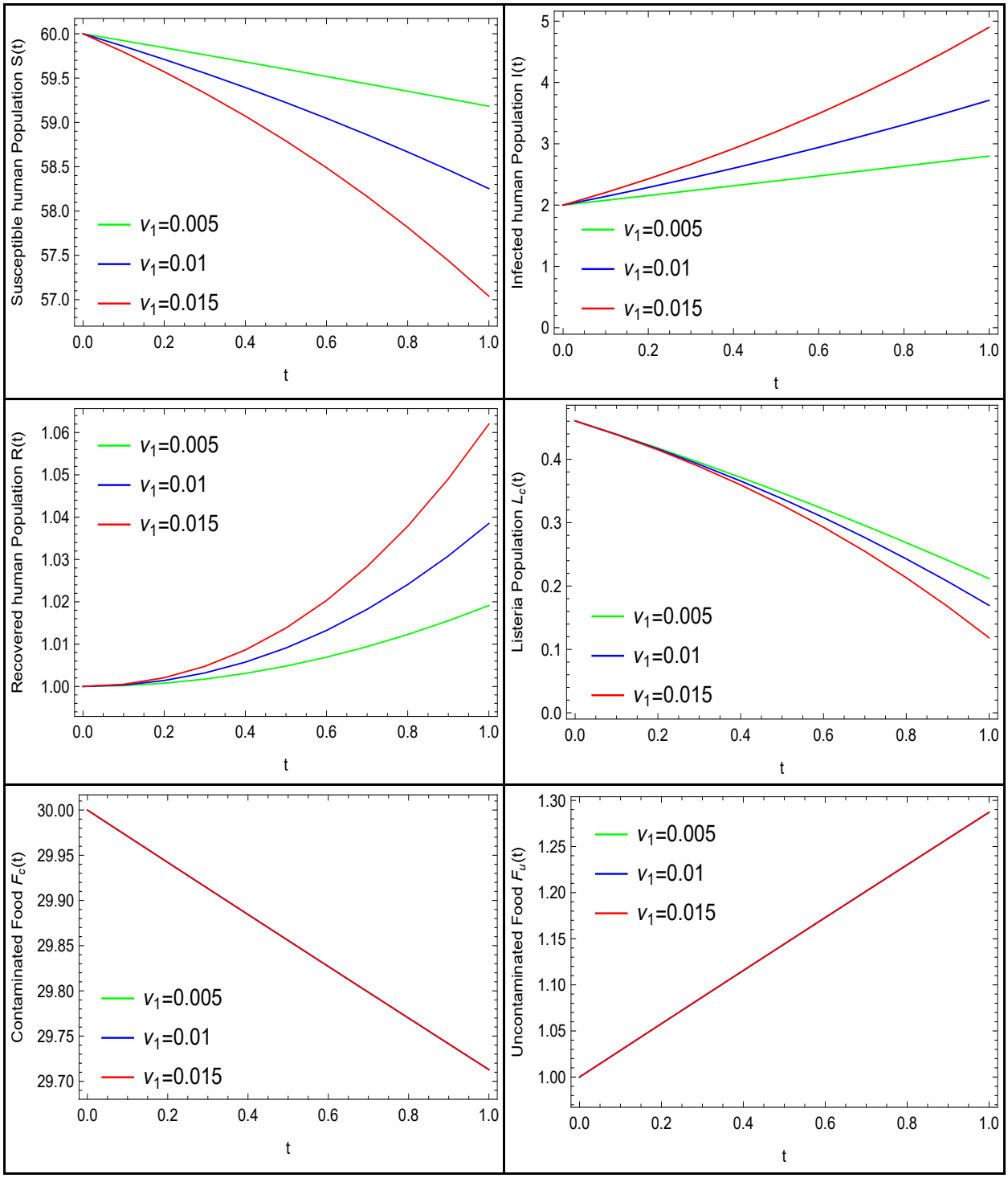

Figure 6.21: Nature of the model with the increase in ν_1, the infection rate.

The effect of the direct infection transmission rate, ν_1, is presented in Figure 6.21. The graphical results suggest that increasing ν_1 leads to a decrease in the susceptible and environmental Listeria populations, while the infected and recovered populations increase. The food

compartments remain unchanged throughout the analysis.

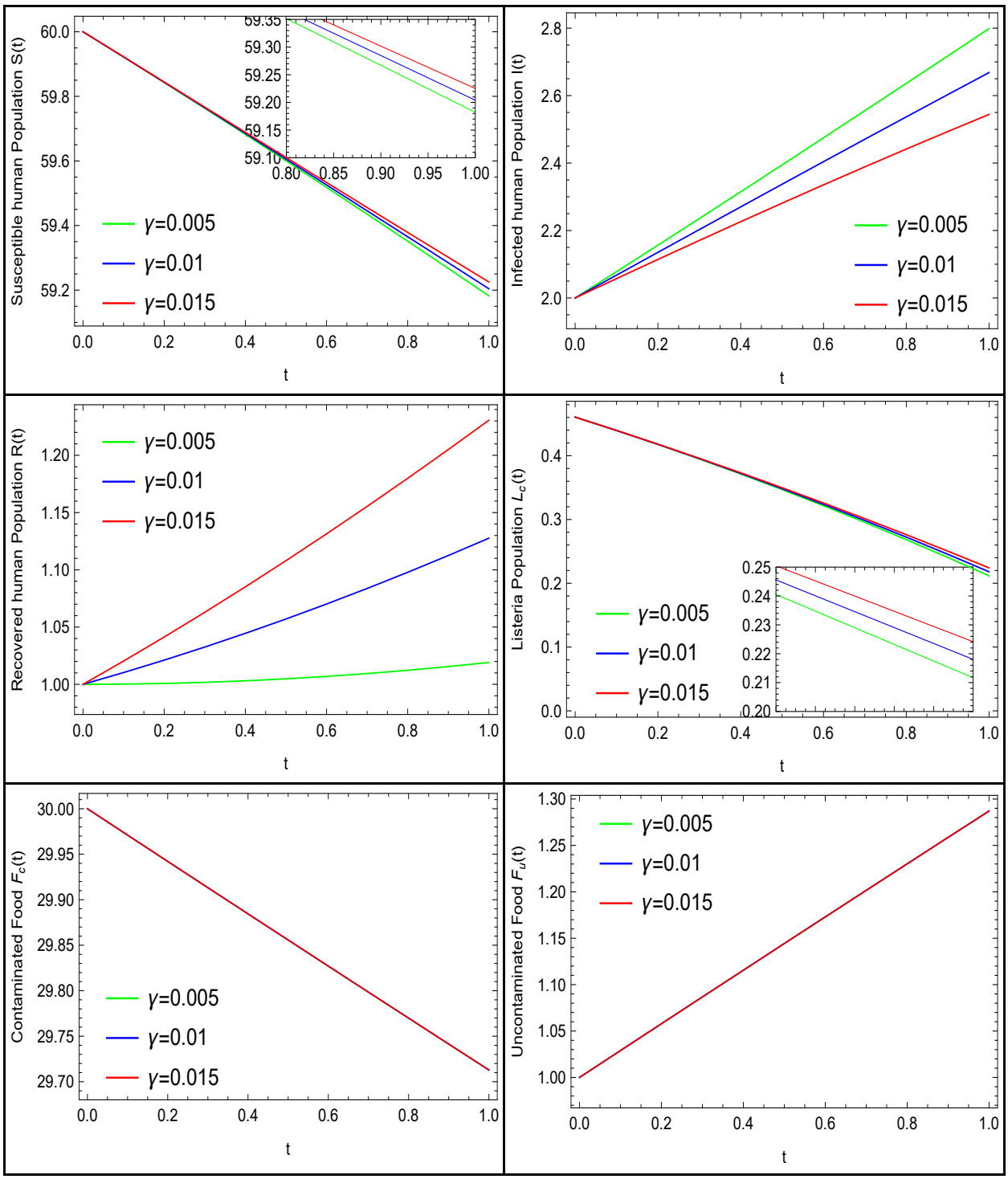

Figure 6.22: Nature of the model with the increase in γ, the recovery rate.

Figure 6.22 illustrates the impact of the recovery rate, γ, on the model dynamics. As the recovery rate increases, the susceptible, recovered, and environmental Listeria populations increase, whereas the infected population decreases due to the more rapid transition of indi-

viduals into the recovered class. The food compartments are not significantly affected.

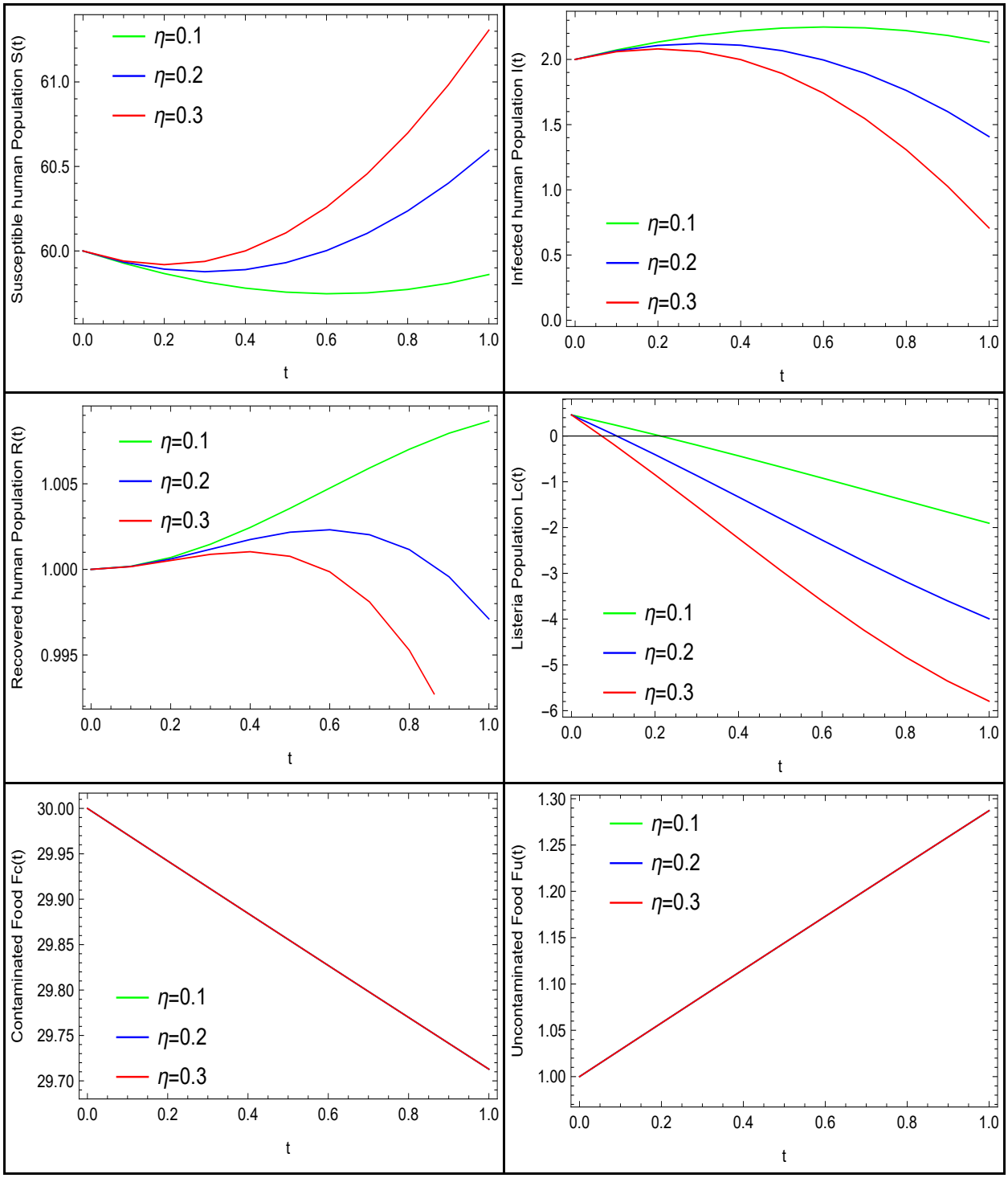

Figure 6.23: Nature of the model with the increase in η, the growth rate of L_c.

The influence of the environmental bacterial growth rate, η, is shown in Figure 6.23. The results reveal that increasing η increases the susceptible population, while the infected, recovered, and environmental Listeria populations decrease. Similar to the previous cases, the

contaminated and uncontaminated food compartments remain unchanged.

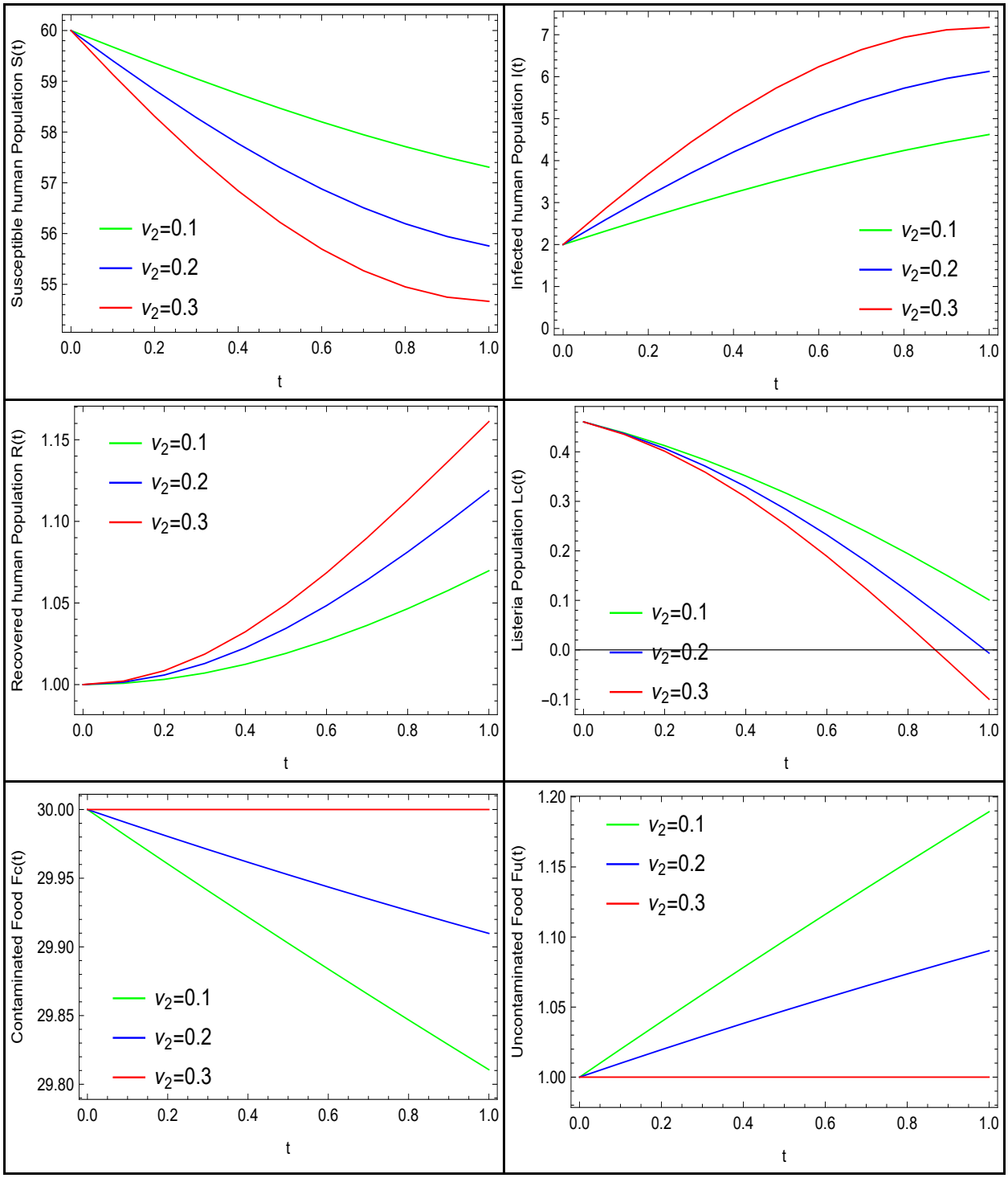

Figure 6.24: Nature of the model with the increase in ν_2, the infection rate of L_c to S.

Figure 6.24 investigates the effect of the infection transmission rate from the environmental bacterial reservoir to susceptible individuals, ν_2. The results indicate that higher values of ν_2 increase the infected and recovered populations and the concentration of contaminated food.

In contrast, the susceptible population, environmental Listeria population, and uncontaminated food compartment decrease as the transmission rate increases.

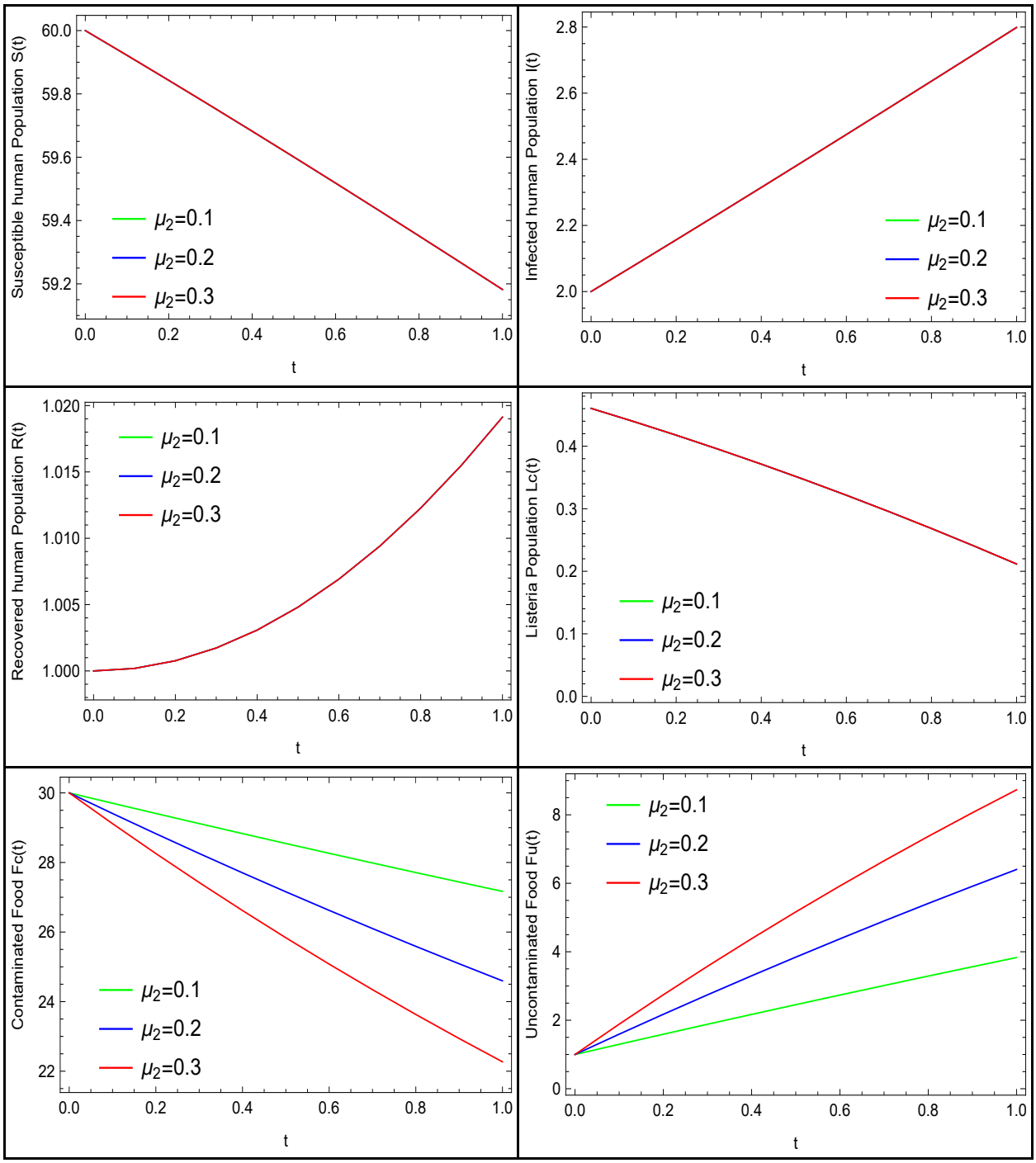

Figure 6.25: Nature of the model with the increase in μ_2, the convergence rate from uncontaminated food to contaminated food.

Finally, Figure 6.25 illustrates the effect of the food decontamination rate, μ_2. Variations in this parameter have no significant impact on the human population compartments or the environmental Listeria population. However, an increase in μ_2 leads to a rise in the uncon-

taminated food population and a corresponding decline in the contaminated food population, reflecting the enhanced effectiveness of decontamination processes.

7 Conclusion

In this work, we examined Listeria infection in pre-cooked packaged food models of fractional order using two different methods: the Homotopy analysis approach and the Runge-Kutta method. We quantitatively examined susceptible, infected, and recovered human populations and Listeria populations, considering contaminated and uncontaminated food, and discussed the impact of various parameters. HAM is a semi-analytical method that yields the analytical solution of a given model under certain additional deformations. Tables 1-13 provide numerical representations of the obtained solutions. Figures 1-18 demonstrate the approaches' performance, while Figures 19-25 indicate the model's nature with different parameters. The results are compared with those of the ND Solver and the Runge-Kutta technique. This study demonstrates that HAM delivers solutions with greater accuracy than the Runge-Kutta technique.

Declarations

Availability of data and materials

The data supporting this study's findings are available within the article.

Funding

No funding was received for this work.

Authors' contributions

All authors contributed equally and significantly to writing this paper. Suguntha Devi K and Sachin K N conducted the literature survey, derived the algorithm, wrote the original draft, and implemented the codes for HAM. Kumbinarasaiah S implemented the codes and revised the final draft of the manuscript. All authors read and approved the final manuscript.

Conflict of interest

The authors declare that they have no conflicts of interest regarding the publication of this paper.

Acknowledgements

The authors would like to thank the anonymous reviewers for their valuable suggestions, which enhanced the quality of this work.

References

[1] O. Mejlholm and P. Dalgaard, *Modeling and predicting the growth boundary of Listeria monocytogenes in lightly preserved seafood*, Journal of Food Protection, **70**(1) (2007), 70–84.

[2] R. Jiang et al., *Modelling the cross-contamination of Listeria monocytogenes in pork during bowl chopping*, International Journal of Food Science & Technology, **53**(3) (2018), 837–846.

[3] K. A. Jackson, M. Iwamoto and D. Swerdlow, *Pregnancy-associated listeriosis*, Epidemiology & Infection, **138**(10) (2010), 1503–1509.

[4] J. A. Lepe, *Current aspects of listeriosis*, Medicina Clínica (English Edition), **154**(11) (2020), 453–458.

[5] C. Shi et al., *Clinical and laboratory characteristics of patients infected by Listeria monocytogenes at a tertiary hospital in Hefei City, China*, Infection and Drug Resistance, (2021), 4409–4419.

[6] F. Duarte et al., *A rare presentation of Listeria monocytogenes infection: perianal abscess associated with lumbar spine osteitis*, IDCases, **15** (2019), e00488.

[7] V. Economou, A. Tsitsos, A. Theodoridis, I. Ambrosiadis and G. Arsenos, *Effects of Chitosan Coatings on Controlling Listeria monocytogenes and Methicillin-Resistant Staphylococcus aureus in Beef and Mutton Cuts*, Applied Sciences, **12**(22) (2022), 11345.

[8] S. T. Duze, M. Marimani and M. Patel, *Tolerance of Listeria monocytogenes to biocides used in food processing environments*, Food Microbiology, **97** (2021), 103758.

[9] B. Giménez et al., *Treatment of beef with gaseous ozone: Physicochemical aspects and antimicrobial effects on heterotrophic microflora and Listeria monocytogenes*, Food Control, **121** (2021), 107602.

[10] S. H. Roh et al., *Inactivation of Escherichia coli O157:H7, Salmonella, Listeria monocytogenes, and Tulane virus in processed chicken breast via atmospheric in-package cold plasma treatment*, LWT, **127** (2020), 109429.

[11] J. K. K. Asamoah et al., *A fractional mathematical model for listeriosis infection using two kernels*, Decision Analytics Journal, **6** (2023), 100191.

[12] A. G. Massia et al., *Prior freezing impact on the growth kinetics of Listeria monocytogenes in hot dog sausages*, Food Control, **157** (2024), 110186.

[13] L. Zhang et al., *Survival and predictive modeling of Listeria monocytogenes under simulated human gastric conditions in the presence of bovine milk products*, International Journal of Food Microbiology, **396** (2023), 110201.

[14] M. Cevikbas, G. Kaiser and S. Schukajlow, *A systematic literature review of the current discussion on mathematical modelling competencies: State-of-the-art developments in conceptualizing, measuring, and fostering*, Educational Studies in Mathematics, **109**(2) (2022), 205–236.

[15] S. Banerjee, *Mathematical modeling: models, analysis, and applications*, Chapman and Hall/CRC, 2021.

[16] L. Ait Mahiout et al., *Mathematical modeling of respiratory viral infection and applications to SARS-CoV-2 progression*, Mathematical Methods in the Applied Sciences, **46**(2) (2023), 1740–1751.

[17] G. Manohara and S. Kumbinarasaiah, *A robust numerical approach for the fractional Polio model by the Genocchi wavelet collocation method*, Journal of Computational and Nonlinear Dynamics, **20**(4) (2025).

[18] S. Kumbinarasaiah and R. Yeshwanth, *Haar wavelet approach for the mathematical model on hepatitis B virus*, J. Comput. Nonlinear Dyn., **19** (2024), 091003-1.

[19] S. Paul et al., *Dynamical behavior of a fractional order SIR model with stability analysis*, Results in Control and Optimization, **10** (2023), 100212.

[20] A. Omame et al., *A fractional-order multi-vaccination model for COVID-19 with non-singular kernel*, Alexandria Engineering Journal, **61**(8) (2022), 6089–6104.

[21] S. Rezapour et al., *A mathematical approach for studying the fractal-fractional hybrid Mittag-Leffler model of malaria under some control factors*, AIMS Math, **8**(2) (2023), 3120–3162.

[22] S. K. N. Sachin, K. Suguntha and S. Kumbinarasaiah, *A semi-analytic and numerical approach to the fractional differential equations*, Iranian Journal of Numerical Analysis and Optimization, **14**(4) (2024), 1069–1105.

[23] Sachin K N, Suguntha Devi K and Kumbinarasaiah S, *A study on the Fractional Ebola Virus Model by the semi-analytic and numerical approach*, Computational Methods for Differential Equations, (2024).

[24] S.-J. Liao, *The proposed homotopy analysis technique for the solution of nonlinear problems*, PhD Thesis, Shanghai Jiao Tong University, 1992.

[25] S. Liao, *An explicit, totally analytical approximate solution for Blasius equation*, Int. J. Non-Linear Mech., **34** (1999), 759–778.

[26] S. Liang and D. J. Jeffrey, *Comparison of homotopy analysis method and homotopy perturbation method through an evolution equation*, Communications in Nonlinear Science and Numerical Simulation, **14**(12) (2009), 4057–4064.

[27] M. Sajid and T. Hayat, *Comparison of HAM and HPM methods in nonlinear heat conduction and convection equations*, Nonlinear Analysis: Real World Applications, **9**(5) (2008), 2296–2301.

[28] Y. Chen, M. Yi and C. Yu, *Error analysis for numerical solution of fractional differential equation by Haar wavelets method*, Journal of Computational Science, **3**(5) (2012), 367–373.

[29] J. P. Chauhan, S. R. Khirsariya, B. M. Yeolekar and M. A. Yeolekar, *Fractional mathematical model of Listeria infection caused by pre-cooked package food*, Results in Control and Optimization, **14** (2024), 100371.

[30] M. Zurigat et al., *The homotopy analysis method for handling systems of fractional differential equations*, Applied Mathematical Modelling, **34**(1) (2010), 24–35.

[31] S. Kumbinarasaiah and M. P. Preetham, *A Study on homotopy analysis method and clique polynomial method*, Computational Methods for Differential Equations, **10**(3) (2022), 774–788.

[32] Z. M. Odibat, *A study on the convergence of homotopy analysis method*, Applied Mathematics and Computation, **217**(2) (2010), 782–789.

[33] S. Liao, *Beyond perturbation: introduction to the homotopy analysis method*, CRC Press, 2003.

[34] S. Liao, *Homotopy analysis method in nonlinear differential equations*, Higher Education Press, Beijing, 2012.

[35] S. Liao, *Advances in the homotopy analysis method*, World Scientific, 2013.